Spectral properties of binary asteroids

Myriam Pajuelo, Mirel Birlan, Benoit Carry, Francesca Demeo, Richard P Binzel, Jérôme Berthier

Monthly Notices
of the
ROYAL ASTRONOMICAL SOCIETY

MNRAS **00,** 1 (2018)
Advance Access publication 2018 April 24

doi:10.1093/mnras/sty1013

Spectral properties of binary asteroids

Myriam Pajuelo,[1,2★] Mirel Birlan,[1,3] Benoît Carry,[1,4] Francesca E. DeMeo,[5] Richard P. Binzel[1,5] and Jérôme Berthier[1]

[1]*IMCCE, Observatoire de Paris, PSL Research University, CNRS, Sorbonne Universités, UPMC Univ Paris 06, Univ. Lille, France*
[2]*Sección Física, Departamento de Ciencias, Pontificia Universidad Católica del Perú, Apartado 1761, Lima, Perú*
[3]*Astronomical Institute of the Romanian Academy, 5 Cutitul de Argint, 040557 Bucharest, Romania*
[4]*Observatoire de la Côte d'Azur, Université Côte d'Azur, CNRS, Lagrange, France*
[5]*Department of Earth, Atmospheric, and Planetary Sciences, Massachusetts Institute of Technology, 77 Massachusetts Avenue, Cambridge, MA 02139, USA*

Accepted 2018 April 16. Received 2018 April 10; in original form 2017 December 21

ABSTRACT

We present the first attempt to characterize the distribution of taxonomic class among the population of binary asteroids (15 per cent of all small asteroids). For that, an analysis of 0.8–2.5 μm near-infrared spectra obtained with the SpeX instrument on the NASA/IRTF is presented. Taxonomic class and meteorite analogue is determined for each target, increasing the sample of binary asteroids with known taxonomy by 21 per cent. Most binary systems are bound in the S, X, and C classes, followed by Q and V types. The rate of binary systems in each taxonomic class agrees within uncertainty with the background population of small near-Earth objects and inner main belt asteroids, but for the C types which are under-represented among binaries.

Key words: methods: observational – techniques: spectroscopic – surveys – meteorites, meteors, meteoroids – minor planets, asteroids: general.

1 INTRODUCTION

Asteroids are leftovers from the formation of the Solar system. As witnesses from the early stages of its formation, a wealth of information is still present among this population. Their study is of prime importance in understanding planetary formation and evolution processes (Bottke et al. 2002). First and foremost, this requires a reliable knowledge of their physical properties in addition to their surface composition and dynamics. Analysis of these parameters can provide relevant information about their relationships and formation scenarios (DeMeo & Carry 2014).

Current understanding of asteroid compositions is derived using a wide range of techniques including visible, near-infrared (NIR), and mid-infrared (mid-IR) photometry, spectroscopy, and polarimetry with ground-based and space telescopes, although most compositional information has derived from visible and NIR spectroscopy and its comparison with that of meteorites in the laboratory (Vernazza et al. 2010). Asteroid classification is thus presently based mainly on spectral features (see DeMeo et al. 2009) which reveal solely the very upper layer of the whole body, which may or may not be representative of the overall composition of the body (Carry 2012). Moreover, if about 18 of the 24 classes in the Bus–DeMeo classification have a mineralogical interpretation (Vernazza et al. 2015, 2016), the composition of the remaining classes is still unknown due to a lack of unambiguous absorption features in the visible and NIR spectra of these bodies.

There are about 750000 known asteroids, most of them belonging to the Main Belt. Among small asteroids (up to 10–15 km), about 15 ± 4 per cent are binary asteroids (Margot et al. 2015), based on the current census of 213 known systems. Unfortunately, spectral classification is missing for 127 (60 per cent) of them (Johnston 2016), and the density has been estimated for 54 (25 per cent) only. It is crucial to gather spectral classifications of these minor bodies, as well as to monitor the relative position of the satellites around them to derive their density (e.g. Carry et al. 2015). This will help us to better constrain the properties of these minor bodies, such as internal structure and formation processes (e.g. Walsh & Jacobson 2015; Scheeres et al. 2015).

In most small binary asteroid systems, the primary component is indeed rapidly rotating and has a high angular momentum (Pravec & Harris 2007), which is not compatible with formation scenarios implying catastrophic impacts. The formation of satellites of small asteroids is more likely linked with YORP-induced spin-up, rotational fission, and mass shedding (Margot et al. 2002; Pravec & Harris 2007; Walsh, Richardson & Michel 2008; Walsh & Jacobson 2015; Margot et al. 2015). In this hypothesis, an asteroid rotates so fast that the centrifugal accelerations surpass the gravitational accelerations that holds the small asteroid together (Weidenschilling 1980). Because the YORP effect is relevant on small asteroids (Pravec et al. 2008; Vokrouhlický et al. 2015), it was sug-

★ E-mail: myriam.pajuelo@obspm.fr

gested by Bottke et al. (2002) to explain the formation of small binary systems by spin-up and mass shedding.

In this article, we aim at increasing the sample of binary asteroids with known spectra, and investigate whether they are more frequent among some taxonomic classes (for instance, the fresh Q-types surfaces compared to the space weathered S types), as predicted from a formation mechanism that involves YORP-induced rotational fission spin-up and mass.

2 OBSERVATIONS AND DATA REDUCTION

The asteroids were observed on 2015 September 29/30 and 2017 January 3 in the 0.8–2.5 μm spectral region with SpeX, the low- to medium-resolution NIR spectrograph and imager (Rayner et al. 2003), on the 3-mNASA IRTF located on Mauna Kea, Hawaii. Observations were performed remotely from the *Centre d'Observation à Distance en Astronomie à Meudon* (CODAM, Birlan et al. 2004, 2006) using the low-resolution Prism mode (R= 100) of the spectrograph. We used a 0.8 × 15 arcsec slit oriented North–South.

We observe the asteroids and solar analogues (used for telluric corrections and removal of the solar continuum) alternatively during the run and close to the meridian. The search for these stars was done with the star locator on the IRTF webpage.[1] The photometrical G2V standards were chosen, with the following stars used as solar analogues: HD 377, HD 7983, and HD 232824, each of them close to their respective asteroid (see details in Table1).

The spectra were obtained alternatively on two separated locations on the slit denoted A and B using the *nodding* procedure (Nedelcu et al. 2007). We follow the *SpeX Observing Manual* (Rayner 2015) throughout the run. We used SPEXTOOL (SPectral EXtraction TOOL), an Interactive Data Language (IDL)-based data reduction package written by Cushing, Vacca & Rayner (2004) to reduce data obtained with SpeX.

The circumstances of observations are presented in Table 1. All the asteroid spectra were obtained taking images with an integration time (IT) of 120s in the nodding procedure for several cycles,[2] in order to increase the signal-to-noise ratio (S/N). For asteroids (2691) Sérsic and (8373) Stephengould, the atmospheric conditions and their low brightness imply a poor S/N. The weather conditions of the night were: seeing 0.6 arcsec, humidity (at the beginning of the run) 16 per cent, we note the presence of clouds during the run and temperature of 4.5 ^{o}C.

The first five targets presented in Section 4 were obtained from 19 h granted by IRTF. Unfortunately, 12 h were lost due to a snow storm at Mauna Kea. To increase the statistics, we also study here the public[3] spectra of 19 binary systems observed within the *MIT–UH–IRTF Joint Campaign for NEO Spectral Reconnaissance*, an ongoing joint observing program for routine measurement of near-Earth object (NEO) spectra being conducted by MIT, the University of Hawaii, and the IRTF on Mauna Kea, Hawaii (Binzel et al. 2006). While taxonomic classification has been performed previously for some of them, we classify again all these spectra with the same protocol as described below (Section 3) for consistency.

[1] http://irtfweb.ifa.hawaii.edu/cgi-bin/spex/find_a0v.cgi
[2] A cycle commands a beam-switch sequence, in which two images are taken for the A and B positions, respectively.
[3] http://smass.mit.edu/minus.html

3 METHODS OF ANALYSIS

Since the first taxonomies in the 1970s, the presence or absence of an absorption band around 1 μm has been the main separator of spectral classes. For those in the S-complex, and for the rarer A and V types, this band is due to pyroxenes and olivine on the surface. The depth of this band is crucial to distinguish the different classes, in particular to distinguish between the space weathered S-type and fresh Q-type spectra (although other parameters such as the band centre and width can be used, see DeMeo, Binzel & Lockhart 2014a). Because it cannot be measured from IR-only spectra, we combine our spectra with their visible counterpart whenever available: a spectrum for (8373) Stephengould (de León et al. 2010) and Sloan Digital Sky Survey (SDSS) colours for (4383) Suruga (Ivezić et al. 2001; DeMeo & Carry 2013). For the other cases, the slope was computed for the spectra normalized to 1.25 μm.

We also compile published spectral, physical, and dynamical properties of the binary asteroids we observed. We summarize them in Table 2, together with the taxonomic classification given in this work. A detailed spectral analysis of each asteroid is presented in Appendix A.

All the analysis of spectra in this work was performed using `M4AST` (Modelling for asteroids), a public software tool developed at the IMCCE (Popescu, Birlan & Nedelcu 2012) and proposed as a centralized data base for published data. It currently contains more than 7000 spectra of asteroids including SMASS MIT's data base (Binzel et al. 2004) and libraries such as RELAB (Pieters & Hiroi 2004). `M4AST` also proposes methods and routines to achieve taxonomy classification, spectral comparison using Cloutis et al. (1986) model to compute spectral parameters, and space weathering effects model proposed by Brunetto et al. (2006) in order to model spectra and extract several mineralogical parameters (Birlan et al. 2016). `M4AST` is free and available via a web interface.[4] To classify the asteroids, we use the χ^2 minimization method with Bus–DeMeo taxonomy (DeMeo et al. 2009). With each classification, `M4AST` gives a reliability factor, a parameter that is defined as the ratio of the number of points of the asteroid spectrum over the total number of points defined for the taxonomic type (Popescu et al. 2012). When comparing with samples from RELAB data base with `M4AST`, we also use the χ^2 metric.

For completeness and whenever possible, we also check the taxonomy with MIT's online classification system,[5] although this tool only returns a definitive classification when a spectrum contains both visible and NIR data. When only NIR observations are analysed, the classification system returns a variety of possible subclasses.

4 RESULTS

All spectra normalized to 1.25 μm are plotted in Fig. 1 with their measurement uncertainty. The results for taxonomic classification of spectra are synthesized in Table 2 to allow a comparison with the physical properties and previously taxonomic classification. Table 3 summarizes the comparison of the observed asteroid spectra with those of meteorites from RELAB data base.[6]

In total, we have determine the taxonomic class of 24 binary asteroids, representing an increase of 21 per cent of the sample of binaries with known taxonomic classification, obtained with the

[4] http://m4ast.imcce.fr/
[5] http://smass.mit.edu/busdemeoclass.html
[6] http://www.planetary.brown.edu/relab/

Table 1. Observational circumstances for the five asteroids observed with SpeX. The asteroid designation, mid-date of observation (Date), apparent magnitude (V), phase angle (α), heliocentric distance (Δ), airmass (AM), integration time for each spectrum (IT), and number of cycles of each observation are presented. The last two columns describe the solar analogues (SA) used for data reduction as well as their airmass at the observing time (AM_{SA}).

Asteroid	Date (UT)	V (mag)	α (°)	Δ (au)	AM	IT (s)	Cycles	SA	AM_{SA}
(2691) Sérsic	2015-09-30T10:10:00.00	16.33	8.69	2.34	1.04	120	6	HD 377	1.21
(4383) Suruga	2015-09-30T12:30:00.00	15.8	5.64	2.30	1.25	120	6	HD 7983	1.41
(7187) Isobe	2015-09-30T14:10:00.00	16.78	30.92	1.77	1.10	120	13	HD 232824	1.22
(8373) Stephengould	2015-09-29T14:38:51.64	17.94	31.20	1.88	1.26	120	3	HD 60298	1.20
(76818) 2000 RG_{79}	2017-01-03T07:20:27.06	16.29	28.25	1.75	1.09	120	3	(SA) 102-1081	1.20

Table 2. For each asteroid, we list its dynamical type (DT), absolute magnitude (H), geometric albedo (p_v) effective diameter in km (D), and any previous report of taxonomy (see Appendix A for all the references), together with the taxonomy and meteorite analogue determined here.

Asteroid	DT	H	p_v	D	Prev tax	Our tax	Meteorite class
(2691) Sérsic	IMB	13.4	0.261 ± 0.062	5 ± 0.11	–	Sr	OC/LL4
(4383) Suruga	MB	12.9	0.320 ± 0.038	6.33 ± 0.09	V	V	AC/HED
(7187) Isobe	HUN	13.89	0.134 ± 0.104	6.05 ± 1.46	–	K	CC/OC
(8373) Stephengould	MC	13.8	–	∼5.29	–	D	IA/CC
(76818) 2000 RG_{79}	HUN	13.7	0.43	∼3.6	–	Xe	EC
(190208) 2006 AQ	AMO	18.1	–	1.06	–	K, Cg	C/CC/OC
(348400) 2005 JF_{21}	AMO	17.1	∼0.59	0.3	–	V	AC/HED
(399307) 1991 RJ_2	AMO	18.9	–	∼0.5	–	T	CC/CM
1994 XD	APO	19.11	–	0.6 ± 0.15	–	S	OC/L5
2014 WZ_{120}	APO	20.44 ± 0.36	–	∼0.3	–	Sv	OC/H5
(410777) 2009 FD	APO	22.1	–	0.15	–	C	EC/CC
(452561) 2005 AB	AMO	17.5	0.03	>1.9	–	Xk	CC/EC
(162000) 1990 OS	APO	19.3	–	0.3 ± 0.02	–	S	Ol/OC/CC
(66063) 1998 RO_1	ATE	18.1	0.14 ± 0.06	0.8 ± 0.15	–	S	OC/L5
(88710) 2001 SL_9	APO	17.6	–	∼0.8	Sr, Q	Sr	OC/LL4
(162483) 2000 PJ_5	ATE	18.41 ± 0.05	0.2 ± 0.05	$\sim 0.6 \pm 0.1$	O, Q	Q	OC/H4
(374851) 2006 VV_2	APO	16.6 ± 0.2	–	1.06 ± 0.05	V,S,A Q,T	L, Xe, Ch	OC/L5
(399774) 2005 NB_7	APO	18.933 ± 0.545	–	0.5 ± 0.1	Sq	S Sq, S, Q	OC/L6
2007 DT_{103}	APO	19.2	–	0.3	Q	Q, Sq, S	OC/LL
(8306) Shoko	MB	4.9	–	3.21	Sq	Q Sq S	OC/LL
(185851) 2000 DP_{107}	APO	18.2	0.15 ± 0.065	0.8 ± 0.16	C, X, Sq	K, Xk Cg	0C/EC/CC
(153591) 2001 SN_{263}	AMO	16.861 ± 0.805	0.048 ± 0.015	2.6	B	C Cb	CC/AC/EC
(285263) 1998 QE_2	AMO	17.07 ± 0.67	0.05 ± 0.03	3.2 ± 0.3	Ch	X, T, D	CC/Sulfide
(481532) 2007 LE	APO	19.7	–	0.5	S	D	Stony Iron/Pallasite

same telescope, the same instrument (SpeX/IRTF), and the same spectral classification standard (DeMeo et al. 2009) and technique (M4AST). Most of these systems are located in the inner main belt (IMB) and near-Earth and Mars-crossing space, while the statistics decrease in the outer belt and Trojan space (Fig.2). In the outer regions of the belt, the sample is dominated by large asteroids with small moons, which are thought to originate from large impacts (e.g. Margot et al. 2015; Pajuelo et al. 2018), while we concentrate here below on the larger population of small binary asteroids, thought to originate from rotation fission (Walsh & Jacobson 2015).

From this larger sample of binary asteroids with known taxonomic class, we study how they distribute over taxonomic classes. Most binary asteroids are found S, X, and C types, following the general trend of main-belt and near-Earth asteroids (NEA, Binzel et al. 2004; DeMeo & Carry 2014; Carry et al. 2016), followed by Q and V types (Fig.3). In the following, we restrict our analysis to the NEA and IMB populations of binary asteroids only. Indeed, the limited amount of binary asteroids with known taxonomy among Mars Crossers (8) and Hungarias (13) implies large uncertainties on their relative ratio and precludes any interpretation.

To determine whichever a taxonomic class is prominent among binaries, we compare our sample with the background population of near-Earth and Mars-crosser asteroids analysed by Carry et al. (2016) in Fig. 4. These authors have indeed showed that the distribution of taxonomic classes was similar among NEAs and inner belt asteroids, in the size range we consider here. The sample size of binary asteroids remains small, resulting in large (typically 10–15 per cent) uncertainties. Within these uncertainties, the distribution of taxonomic classes of binary asteroids is extremely similar to the background population but for C types in the main belt. This lack of any C-type binary in the main belt may be enhanced by the small number statistics, but is supported by the lower rate of C types among binary NEAs with respect to the background.

A couple of other marginal mismatches can be highlighted: the X and Q types among NEAs and V types in the main belt. While these discrepancies are small, the close agreement for all other classes (including the rarer B, K, and L types) points to genuine differences. If an excess of Q types among binary could have be expected, there is only a hint of it in present data. A much larger sample is required to assess the Q/S ratio among binaries, but once achieved, it will provide the relative time-scale of binary formation and space weathering.

The under-representation of C types observed here is counter-intuitive: the strength of YORP is anticorrelated with albedo and

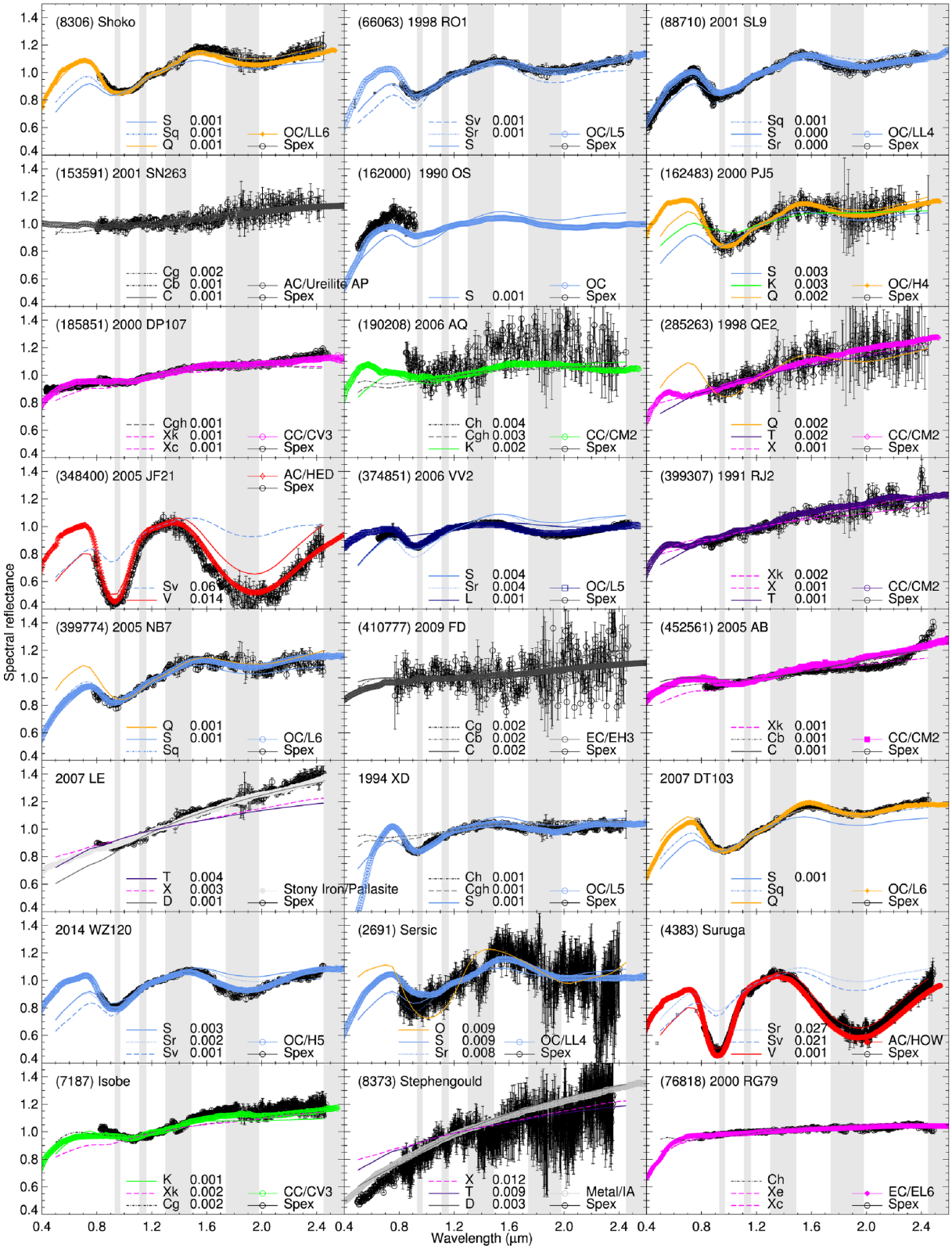

Figure 1. Spectra, normalized to unity at 1.25 μm, of all the binary asteroids presented in this work. The best three matches with Bus–DeMeo taxonomy (DeMeo et al. 2009). are reported with their χ^2. Shaded in light grey are the wavelength ranges most affected by atmospheric absorption (Lord 1992). Colour lines corresponds to the best match spectra from RELAB library.

density, both lower for C types than S types (Mainzer et al. 2011; Carry 2012). Moreover, fission should occur more easily in C types which present a larger macroporosity (Scheeres et al. 2015). Nevertheless, this requires further investigation, increasing significantly

Table 3. Matches for each asteroid with meteorites from RELAB. The comparison was made using a χ^2 method and the selection of results based on spectral features (band, band gap, and concavity) and albedo value. Laser-irradiated samples are marked with a †. The acronyms for the texture are particulate (P), particulate ground (PG), sorted (S), dry-Sieved (D), thin section (TS), and chip (C).

Target	χ^2	Meteorite	Sample ID	Type	Texture	Size (μm)
(2691) Sérsic	0.01339	Los Angeles #1	MT-JLB-006-C	SHE	C	–
	0.01381	Hamlet	OC-TXH-002-A20	OC/LL4	C	–
	0.01491	Soko-Banja	MR-MJG-070	OC/LL4	–	–
	0.01501	Barratta	MH-CMP-002	OC/L4	Slab	–
	0.01512	Bjurbole unshaken	MP-FPF-027	OC/L4	P	0–1000
(4383) Suruga	0.00166	Pavlovka	MR-MJG-094	AC/Howardite	–	–
	0.00197	Le Teilleul	MP-TXH-093-A	AC/HED	P	0–25
	0.00217	Frankfort	MP-TXH-085-A	AC/Howardite	P	0–25
	0.00225	Y-7308,142	MP-TXH-097-A	AC/HED	P	0–25
	0.00229	Kapoeta P11410	SN-CMP-012	AC/HED	TS	–
(7187) Isobe	0.00045	Almahata Sitta #4	MT-PMJ-093-C	AC/UAP	PG	0–125
	0.00046	Allende: HC-10	MT-TJM-073	CC/CV3	PG	0–38
	0.00047	Tsarev	MA-ATB-053	OC/L5	PG	–
	0.00051	LEW87009,16	LM-LAM-011	CC/CK6	TS	–
	0.00052	EET90021,10	MP-TXH-043	CC/C2	P	0–125
(8373) Stephengould	0.00543	TRO201/MET101	SC-EAC-093	IA Metal EC	–	–
	0.00563	MET101	SC-EAC-063	IA Metal	–	–
	0.00601	TRO201	EA-EAC-001-B	Sulfide/Troilite	Slab	<45
	0.00619	Tagish Lake ET01-B	MT-TXH-024	CC/CM	PG	0–125
	0.00637	Butler	MR-MJG-081	Iron	–	–
(76818) 2000 RG_{79}	0.00009	ALHA81021,89	MT-PFV-119-B	EC/EL6	PG	0–25
	0.00010	Mayo Belwa	TB-TJM-046	AC/AEA	PG	0–125
	0.00011	QUE93372,13	MT-PFV-129-B	EC/EH5	PG	0–25
	0.00011	ALH84206,25	MT-PFV-118-A	EC/EH3	PG	0–45
	0.00011	KLE98300,33 (EH3)	MT-PFV-122-A	EC/EH3	PG	0–45
(190208) 2006 AQ	0.00623	Los Angeles #1	MT-JLB-006-B	SHE	C	–
	0.00651	Murchison	MR-MJG-109	CC/CM2	–	–
	0.00658	Athens	OC-TXH-013-A	OC/LL6	C	–
	0.00674	NWA753	TB-TJM-114	C/R	PG	0–125
	0.00682	A-881988,70	MP-TXH-059	C/R	P	0–125
(348400) 2005 JF_{21}	0.00468	Kapoeta	MP-TXH-053	AC/Howardite	–	0–1000
	0.00567	MIL07001	MT-AWB-168	AC/Diogenite	PG	–
	0.00589	GRA98108,26	RM-REM-125	AC/Diogenite	C	–
	0.00610	Shalka	MR-MJG-101	AC/Diogenite	–	–
	0.00641	Ellemeet	MP-D2M-112	AC/Diogenite	P	–
(399307) 1991 RJ_2	0.00129	Mighei	MA-ATB-072	CC/CM2	P S	–
	0.00135	Mighei	MA-ATB-065	CC/CM†	P S	75–125
	0.00138	Pervomaisky	RS-CMP-064	OC/L6	Slab	–
	0.00138	Mundrabilla	MB-CMP-006-P3	Sulfide/Troilite	P	45–63
	0.00141	Mighei	MA-ATB-064	CC/CM†	P S	40–75
1994 XD	0.00027	Barwise	MR-MJG-036	OC/H5	–	–
	0.00028	LEW86018,71	MT-PFV-130-A	OC/L3.1	PG D	0–45
	0.00033	Aribba	DP-JNG-017	OC/L5	PG S	0–125
	0.00034	Krymka dark powder	RS-CMP-063-D	OC/LL3	P	20–250
	0.00036	Blackwell	MT-HYM-081	OC/L5	PG S	0–150
2014 WZ_{120}	0.00056	Ehole	OC-TXH-006-A40	OC/H5	C	–
	0.00058	Zhovtnevyi	MR-MJG-041	OC/H5	–	–
	0.00065	Allegan	TB-TJM-125	OC/H5	PG	0–150
	0.00066	Magombedze	TB-TJM-108	OC/H5	PG	0–150
	0.00067	Lancon	MR-MJG-033	OC/H6		–
(410777) 2009 FD	0.00703	KLE98300,33	MT-PFV-122-B	EC/EH3	PG D	0–25
	0.00706	Y-82162,79	MB-CMP-019-A	CC/CI	PG S	0–125
	0.00718	Almahata Sitta	MT-PMJ-093	AC/Ureilite	C #4	–
	0.00724	EET96135,20	MT-PFV-120-A	EC/EH4/5	PG D	0–45
	0.00725	El-Quss Abu Said	MP-KHO-131-A	CC/CM2	PG D	0–125

Table 3 *– continued*

Target	χ^2	Meteorite	Sample ID	Type	Texture	Size (μm)
(452561) 2005 AB	0.00102	Almahata Sitta	MT-PMJ-098	AC/Ureilite	C #47	–
	0.00122	Rose City	MR-MJG-079	OC/H5	Slab	–
	0.00124	Abee 900C	MT-TXH-040-F	EC/E4	P	0–125
	0.00127	Y-74659	MB-TXH-087-C	AC/Ureilite	P	45–75
	0.00130	Murchison	MH-FPF-052-A	CC/CM2	P	0–90
(162000) 1990 OS	0.00073	Sahara 99555	TB-TJM-057	AC/Angrite	PG	0–125
	0.00075	ALHA77005	DD-MDD-009	Olivine	PG	0–50
	0.00075	Leoville	MR-MJG-120	CC/CV3	–	–
	0.00079	EET87860,14	LM-LAM-012	CC/CK5-6	TS	–
	0.00080	Campo de Cielo	TB-TJM-059	Si Inclusion	PG	0–125
(66063) 1998 RO_1	0.00019	Malakal	TB-TJM-109	OC/L5	PG	0–150
	0.00020	Y-74191	MB-TXH-084-A	OC/L3	P	0–25
	0.00022	Paranaiba	MB-CMP-010-L	OC/L6	P	25–250
	0.00022	Kuttippuram	TB-TJM-098	OC/L6	PG	0–75
	0.00023	Mirzapur	TB-TJM-111	OC/L5	PG	0–150
(88710) 2001 SL_9	0.00059	Hamlet	OC-TXH-002-C	OC/LL4	PG S	0–125
	0.00064	Chateau Renard	OC-TXH-011-D15	OC/L6	PG S	0–125
	0.00116	Dhajala	DP-JNG-012	OC/H3.4	PG S	0–125
	0.00128	Hamlet #1	MR-MJG-069	OC/LL4	–	–
	0.00137	Tsarev 15384,3-2	RS-CMP-065-T	OC/L5	TS	–
(162483) 2000 PJ_5	0.00165	Quenggouk	MR-MJG-042	OC/H4	–	–
	0.00176	Bandong	TB-TJM-067	OC/LL6	PG	0–150
	0.00179	Jelica	MR-MJG-072	OC/LL6	–	–
	0.00180	Leedey	MR-MJG-060	OC/L6	–	–
	0.00185	NWA1948	OC-SXS-023-D	OC/LL6	PG S	0–250
(374851) 2006 VV_2	0.00035	Farmington	MR-MJG-077	OC/L5	–	–
	0.00037	Almahata Sitt	MT-PMJ-110	AC/Ureilite	C #51	–
	0.00039	Dhajala	DP-JNG-011	OC/H3.4	PG S	0–125
	0.00040	Novosibirsk	RS-CMP-049-L	OC/H5-6	P	20–250
	0.00047	Mezo-Madaras	MR-MJG-043	OC/L3	–	–
(399774) 2005 NB_7	0.00080	Chateau Renard	OC-TXH-011-D35	OC/L6	PG	0–125
	0.00099	EETA79001,73	LM-LAM-007-73	SHE	TS	–
	0.00116	LEW85332,48	MT-EKT-017	CC/C3	PG	0–125
	0.00129	Appley Bridge	OC-TXH-012-A40	OC/LL6	C	–
	0.00134	Tsarev 15384,3-2	RS-CMP-065-T	OC/L5	TS	–
2007 DT_{103}	0.00012	Chateau Renard	OC-TXH-011-A80	OC/L6†	C	–
	0.00016	Almahata Sitta #44	MT-PMJ-108-B	AC/Ureilite	PG D	125–500
	0.00032	Y-74442	MB-TXH-086-A	OC/LL4	P	0–25
	0.00036	Appley Bridge	OC-TXH-012-A40	OC/LL6	C	–
	0.00056	Y-74646	MB-TXH-085-B	OC/LL6	P	25–45
(8306) Shoko	0.00032	Quenggouk	MR-MJG-042	OC/H4	–	–
	0.00035	Jelica	MR-MJG-072	OC/LL6	–	–
	0.00045	Greenwell Springs	TB-TJM-075	OC/LL4	PG	0–150
	0.00045	Chateau Renard	OC-TXH-011-A20	OC/L6†	C	–
	0.00056	NWA1799 um	OC-SXS-026-D	OC/LL5	PG S	0–250
(185851) 2000 DP_{107}	0.00033	Allende 700C	MB-TXH-063-HD	CC/CV3	PG	0–63
	0.00037	Tsarev	MA-ATB-053	OC/L5†	PG S	–
	0.00053	Orvinio Clast & Melt	MP-DTB-028-C	OC/L6	P	50–250
	0.00057	DaG 1042,05	LM-H1T-052-C	Lunar Breccia	PG D	0–125
	0.00057	Abee 700C	MT-TXH-040-D	EC/E4	P	0–125
(153591) 2001 SN_{263}	0.00120	El-Quss Abu Said	MP-KHO-131-A	CC/CM2	PG D	0–125
	0.00127	Almahata Sitta #4	MT-PMJ-093	AC/Ureilite	C	–
	0.00128	EET96135,20	MT-PFV-120-B	EC/EH4/5	PG D	0–25
	0.00131	Y-82162,79	MB-CMP-019-A	CC/CI	PG S	0–125
	0.00142	KLE98300,33	MT-PFV-122-B	EC/EH3	PG D	0–25
(285263) 1998 QE_2	0.00227	Mighei	MR-MJG-108	CC/CM2	P	0–75
	0.00229	TRO201	SC-EAC-064	Sulfide/Troilite	P	0–45
	0.00234	Mundrabilla	MB-CMP-006-P2	Sulfide/Troilite	P	25–45
	0.00234	Tagish Lake ET01-B	MT-MEZ-011	CC/CI	PG D	0–125
	0.00238	Allende	MS-CMP-040-C	CC/CV3	P	0–75

Table 3 – *continued*

Target	χ^2	Meteorite	Sample ID	Type	Texture	Size (μm)
(481532) 2007 LE	0.00033	Y-8451,20	MB-TXH-039	Pallasite	–	–
	0.00036	ALH84019	TB-TJM-056	Metal/Aubrite	TS	–
	0.00047	Troilite	MI-CMP-011	Sulfide/Troilite	Slab	–
	0.00051	MIX09	SC-EAC-093	TRO201/MET101	P	0–45
	0.00053	Casey County	MR-MJG-080	Iron/Octahedrite	–	–

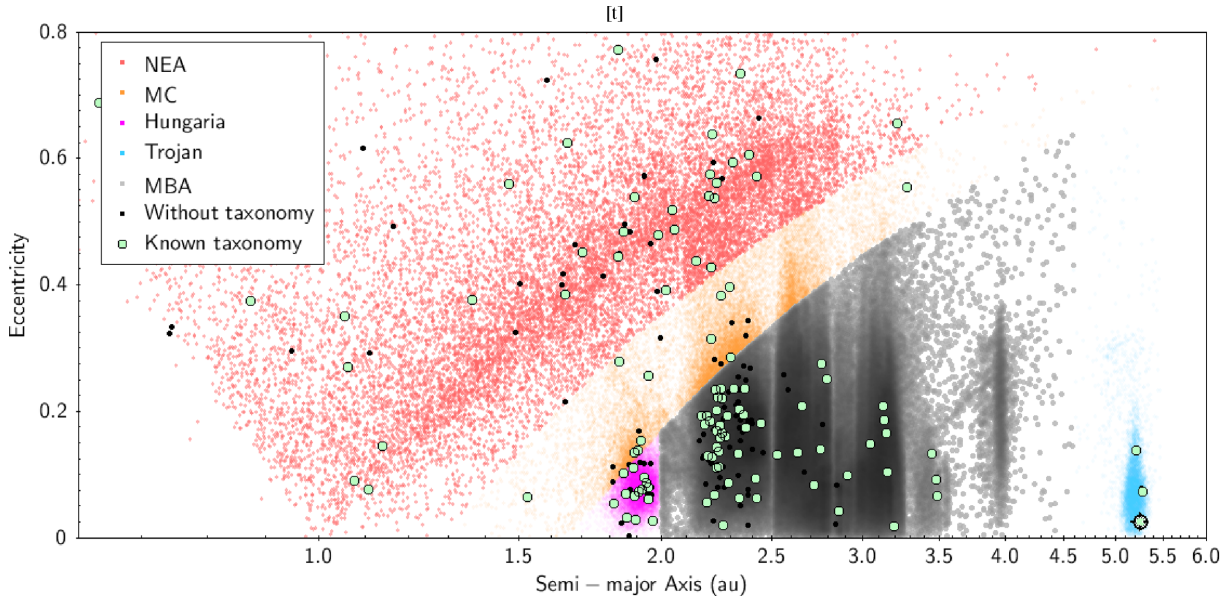

Figure 2. Plot of binaries with known taxonomy (light green dots), and all-binary population (black dots) among the total asteroid population on the background.

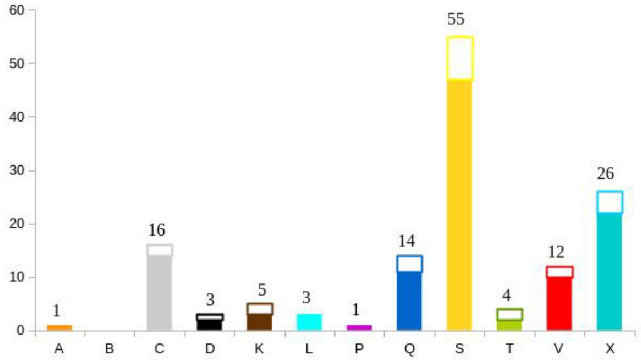

Figure 3. Distribution of taxonomic classes among binary asteroids. Open bars correspond to classifications determined for the first time in this study, and the number to the total.

the number of binaries with taxonomy, to be addressed. The present sample remains limited, and there is a bias against discovering binary C types compared to S types in a magnitude limited survey: YORP effect is strongly dependent on the diameter.

The percentage of remaining binaries without taxonomy among NEAs, MCs, Hungaria, and IMB is 32 per cent, 45 per cent, 39 per cent, and 60 per cent, respectively. While the sample size remains limited, differences between the population of binary and the background asteroids seem to rise. There is hence a clear need for increasing the sample size to address the formation mechanism of satellites of asteroids, by both discovering small binary systems in the middle and outer parts of the belt (not dominated by S-types asteroids), and spectrally characterizing them. The vast catalogues of multifilters sparse photometry from the upcoming large surveys such as *Gaia*, Large Synoptics Survey Telescope, and *Euclid* (Mignard et al. 2007; LSST Science Collaboration et al. 2009; Gaia Collaboration et al. 2016; Carry 2018) offer promising prospects to address this point.

5 CONCLUSIONS

NIR spectroscopy of five binary asteroids was obtained with SpeX/IRTF and combined with 19 additional from the MIT–UH–IRTF Joint Campaign for NEO Spectral Reconnaissance. We determine the taxonomic class and most-likely meteorite analogue for all 24 targets, increasing the sample of binary asteroids with known taxonomy by 21 per cent. Taking into account all systems with known taxonomic type, we compare the distribution of taxonomic classes among near-Earth and inner belt binaries with that of the background population. Both population agrees with uncertainties but for C-types asteroids that are under-represented among binaries, which is unexpected for a formation scenario of satellites of small asteroids by YORP spin-up and rotational fission. The large (typically 10–15 per cent) uncertainty on the distribution of taxonomic class shall however be improved to ascertain this point, based on small statistics. Surveys to discover and characterize small binary systems in the middle and outer belts will help address this point.

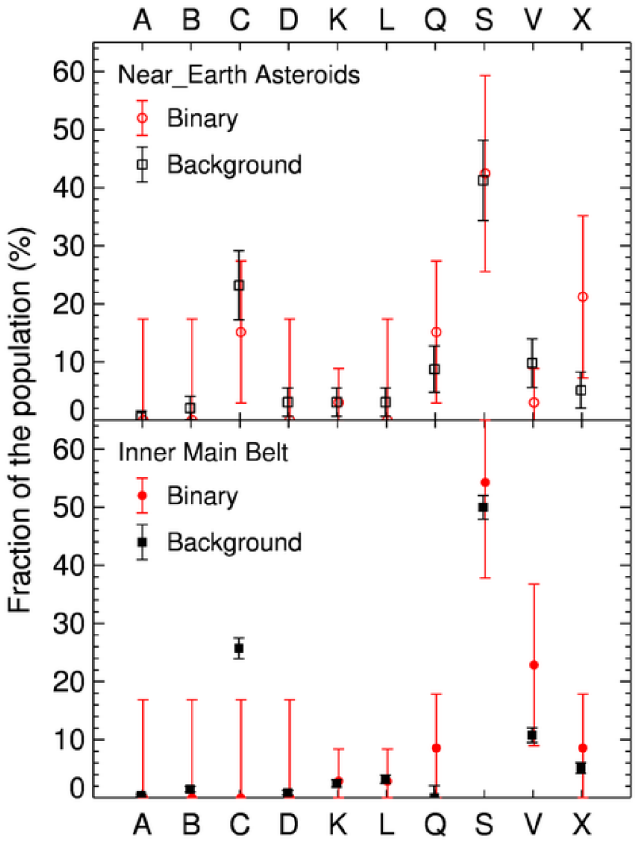

Figure 4. Comparison of the distributions of taxonomic classes between binaries (red symbols) and the background (black) among NEAs (top) and main belt (bottom) populations (taken from DeMeo & Carry 2013; Carry et al. 2016). Uncertainties are taken as the margin of error computed from the sample size.

ACKNOWLEDGEMENTS

5 ACKNOWLEDGEMENTS

This article is based on observations acquired remotely with InfraRed Telescope Facilities from CODAM facilities. We thank the operator at IRTF for his contribution. This research utilizes spectra acquired with the NASA RELAB facility at Brown University. This research has made use of data and services provided by the International Astronomical Union's Minor Planet Center.

M. P. acknowledges funding by the Pontificia Universidad Católica del Perú (PUCP).

The authors acknowledge the use of TOPCAT (Taylor 2005), NEODYS-2 Database (http://Newton.dm.unipi.it/neodys/index.php?pc=0), the use of the Virtual Observatory tools `Miriade`[7] (Berthier et al. 2008), and the Near-Earth Asteroids Data Base service from The European Asteroid Research Node (http://earn.dlr.de/nea/).

The asteroid taxonomy classification based on SDSS observations was obtained from the Planetary Data System.

Part of the data utilized in this publication were obtained and made available by The MIT–UH–IRTF Joint Campaign for NEO Reconnaissance. The IRTF is operated by the University of Hawaii under Cooperative Agreement no. NCC 5-538 with the National Aeronautics and Space Administration, Office of Space Science, Planetary Astronomy Program. The MIT component of this work is supported by NASA grant 09-NEOO009-0001, and by the National Science Foundation under grants nos 0506716 and 0907766.

[7] http://vo.imcce.fr/

REFERENCES

Belskaya I. N., Shevchenko V. G., 2000, Icarus, 147, 94
Berthier J., Hestroffer D., Carry B., Ďurech J., Tanga P., Delbo M., Vachier F., 2008, LPI Contrib., 1405, 8374
Betzler A. S., Novaes A. B., 2009, Minor Planet Bull., 36, 94
Binzel R. P., Rivkin A. S., Stuart J. S., Harris A. W., Bus S. J., Burbine T. H., 2004, Icarus, 170, 259
Binzel R. P., Thomas C. A., DeMeo F. E., Tokunaga A., Rivkin A. S., Bus S. J., 2006, in Mackwell S., Stansbery E., eds, Lunar and Planetary Sci. Conf. Vol. 37
Birlan M., Barucci M. A., Vernazza P., Fulchignoni M., Binzel R. P., Bus S. J., Belskaya I., Fornasier S., 2004, New Astron., 9, 343
Birlan M., Vernazza P., Fulchignoni M., Barucci M. A., Descamps P., Binzel R. P., Bus S. J., 2006, A&A, 454, 677
Birlan M., Popescu M., Irimiea L., Binzel R., 2016, AAS Division for Planetary Sciences Meeting Abstracts, 325.17
Bottke Jr. W. F., Cellino A., Paolicchi P., Binzel R. P., 2002, Asteroids III
Brunetto R., Vernazza P., Marchi S., Birlan M., Fulchignoni M., Orofino V., Strazzulla G., 2006, Icarus, 184, 327
Carry B., 2012, Planet. Space Sci., 73, 98
Carry B., 2018, A&A, 609, A113
Carry B. et al., 2015, Icarus, 248, 516
Carry B., Solano E., Eggl S., DeMeo F. E., 2016, Icarus, 268, 340
Carvano J. M., Hasselmann P. H., Lazzaro D., Mothé-Diniz T., 2010, A&A, 510, A43
Cloutis E. A., Gaffey M. J., Jackowski T. L., Reed K. L., 1986, J. Geophys. Res., 91, 11
Cloutis E. A., Hudon P., Romanek C. S., Bishop J. L., Reddy V., Gaffey M. J., Hardersen P. S., 2010, Meteorit. Planet. Sci., 45, 1668
Cushing M. C., Vacca W. D., Rayner J. T., 2004, PASP, 116, 362
Dandy C. L., Fitzsimmons A., Collander-Brown S. J., 2003, Icarus, 163, 363
de León J., Licandro J., Serra-Ricart M., Pinilla-Alonso N., Campins H., 2010, A&A, 517, A23
de Sanctis M. C., Migliorini A., Luzia Jasmin F., Lazzaro D., Filacchione G., Marchi S., Ammannito E., Capria M. T., 2011, A&A, 533, A77
DeMeo F. E., Carry B., 2013, Icarus, 226, 723
DeMeo F. E., Carry B., 2014, Nature, 505, 629
DeMeo F. E., Binzel R. P., Slivan S. M., Bus S. J., 2009, Icarus, 202, 160
DeMeo F. E., Binzel R. P., Lockhart M., 2014a, Icarus, 227, 112
DeMeo F. E., Binzel R. P., Carry B., Polishook D., Moskovitz N. A., 2014b, Icarus, 229, 392
Dunn T. L., Burbine T. H., Bottke W. F., Clark J. P., 2013, Icarus, 222, 273
Fieber-Beyer S. K., Gaffey M. J., Bottke W. F., Hardersen P. S., 2015, Icarus, 250, 430
Florczak M., Barucci M. A., Doressoundiram A., Lazzaro D., Angeli C. A., Dotto E., 1998, Icarus, 133, 233
Fulchignoni M., Birlan M., Antonietta Barucci M., 2000, Icarus, 146, 204
Gaffey M. J., Burbine T. H., Piatek J. L., Reed K. L., Chaky D. A., Bell J. F., Brown R. H., 1993, Icarus, 106, 573
Gaffey M. J., Cloutis E. A., Kelley M. S., Reed K. L., 2002, Asteroids III, p. 183
Gaia Collaboration et al., 2016, A&A, 595, A1
Gietzen K. M., Lacy C. H. S., Ostrowski D. R., Sears D. W. G., 2012, Meteorit. Planet. Sci., 47, 1789
Hardersen P. S., Gaffey M. J., Abell P. A., 2004, Icarus, 167, 170
Hasselmann P. H., Carvano J. M., Lazzaro D., 2011, NASA Planetary Data System, 145
Hergenrother C. W., Whiteley R. J., Christensen E. J., 2009, Minor Planet Bull., 36, 16
Hicks M., Buratt B., Dalba P., 2013a, Astron. Telegram, 5121
Hicks M., Lawrence K., Chesley S., Chesley J., Rhoades H., Elberhar S., Carcione A., Borlase R., 2013b, Astron. Telegram, 5132

Howell E. S., Magri C., Vervack R. J., Nolan M. C., Fernandez Y., Rivkin A. S., 2008, AAS/Division for Planetary Sciences Meeting Abstracts #40, 436
Ivezić Ž. et al., 2001, AJ, 122, 2749
Ivezić Ž., Juric M., Lupton R. H., Tabachnik S., Quinn T. SDSS Collaboration 2010, NASA Planetary Data System, p. 124
Jagoutz E., Wanke H., 1986, Geochim. Cosmochim. Acta, 50, 939
Johnston W. R., 2016, NASA Planetary Data System, p. 244
Kumar S., Hardersen P. S., Gaffey M. J., 2006, in Mackwell S., Stansbery E., eds, Lunar and Planetary Science Conference Vol. 37
Lazzarin M., Marchi S., Barucci M. A., Di Martino M., Barbieri C., 2004, Icarus, 169, 373
Lazzarin M., Marchi S., Magrin S., Licandro J., 2005, MNRAS, 359, 1575
Lazzarin M., Magrin S., Marchi S., 2008, Mem. Soc. Astron. Ital. Suppl., 12, 20
Lord S. D., 1992, Technical Report, A New Software Tool for Computing Earth's Atmospheric Transmission of Near- and Far-Infrared Radiation. NASA, Washington, DC
LSST Science Collaboration et al., 2009, preprint
Mainzer A. et al., 2011, ApJ, 741, 90
Margot J. L., Nolan M. C., Benner L. A. M., Ostro S. J., Jurgens R. F., Giorgini J. D., Slade M. A., Campbell D. B., 2002, Science, 296, 1445
Margot J.-L., Pravec P., Taylor P., Carry B., Jacobson S., 2015, Asteroids IV, p. 355
Marsset M. et al., 2017, A&A, 604, A64
Masiero J. R., Mainzer A. K., Grav T., Bauer J. M., Cutri R. M., Nugent C., Cabrera M. S., 2012, ApJ, 759, L8
Masiero J. R., DeMeo F. E., Kasuga T., Parker A. H., 2015, Asteroids IV, p. 323
Mignard F. et al., 2007, Earth Moon Planets, 101, 97
Moskovitz N. A., Willman M., Burbine T. H., Binzel R. P., Bus S. J., 2010, Icarus, 208, 773
Moskovitz N. A. et al., 2017, Icarus, 284, 97
Nedelcu D. A., Birlan M., Vernazza P., Descamps P., Binzel R. P., Colas F., Kryszczynska A., Bus S. J., 2007, A&A, 470, 1157
Nedelcu D. A., Birlan M., Popescu M., Bădescu O., Pricopi D., 2014, A&A, 567, L7
Nesvorný D., Morbidelli A., Vokrouhlický D., Bottke W. F., Brož M., 2002, Icarus, 157, 155
Nimura T., Hiroi T., Ohtake M., Ueda Y., Abe M., Fujiwara A., 2006, in Mackwell S., Stansbery E., eds, Lunar and Planetary Science Conference Vol. 37
Pajuelo M. et al., 2018, Icarus, 309, 134
Perna D., Alvarez-Candal A., Fornasier S., Kaňuchová Z., Giuliatti Winter S. M., Vieira Neto E., Winter O. C., 2014, A&A, 568, L6
Pieters C. M., Hiroi T., 2004, in Mackwell S., Stansbery E., eds, Lunar and Planetary Science Conference Vol. 35
Pieters C. M., McFadden L. A., 1994, Ann. Rev. Earth Planet. Sci., 22, 457
Polishook D., Brosch N., 2008, Icarus, 194, 111
Polishook D., Moskovitz N., Binzel R. P., DeMeo F. E., Vokrouhlický D., Žižka J., Oszkiewicz D., 2014, Icarus, 233, 9
Popescu M., Birlan M., Nedelcu D. A., 2012, A&A, 544, A130
Pravec P., Harris A. W., 2007, Icarus, 190, 250
Pravec P., Kusnirak P., Hicks M., Holliday B., Warner B., 2000, IAU Circ., 7504, , #3
Pravec P. et al., 2008, Icarus, 197, 497
Rayner 2015, SpeX Observing Manual. IRTF NASA Infrared Telescope Facility Institute for Astronomy University of Hawai, Available at: http://irtfweb.ifa.hawaii.edu/ spex/SpeX_manual_20mar15.pdf
Rayner J. T., Toomey D. W., Onaka P. M., Denault A. J., Stahlberger W. E., Vacca W. D., Cushing M. C., Wang S., 2003, PASP, 115, 362
Reddy V., 2009, PhD thesis, University of North Dakota, Grand Forks
Rivkin A. S., Binzel R. P., Bus S. J., 2005, Icarus, 175, 175
Scheeres D. J., Britt D., Carry B., Holsapple K. A., 2015, Asteroid Interiors and Morphology. Univ. Arizona Press, Tucson, AZ, p. 745
Spoto F., Milani A., Farnocchia D., Chesley S. R., Micheli M., Valsecchi G. B., Perna D., Hainaut O., 2014, A&A, 572, A100
Sunshine J. M., Pieters C. M., 1993, J. Geophys. Res., 98, 9075
Taylor M. B., 2005, in Shopbell P., Britton M., Ebert R., eds, ASP Conf. Ser. Vol. 347, Astronomical Data Analysis Software and Systems XIV, Astron. Soc. Pac., San Francisco. p. 29
Thomas C. A., Emery J. P., Trilling D. E., Delbó M., Hora J. L., Mueller M., 2014, Icarus, 228, 217
Vereshchagina I. A., 2011, preprint (arXiv:1102.0152)
Vereshchagina I. A., Gorshanov D. L., Devyatkin A. V., Papushev P. G., 2009, Sol. Syst. Res., 43, 291
Vernazza P., Binzel R. P., Thomas C. A., DeMeo F. E., Bus S. J., Rivkin A. S., Tokunaga A. T., 2008, Nature, 454, 858
Vernazza P., Brunetto R., Binzel R. P., Perron C., Fulvio D., Strazzulla G., Fulchignoni M., 2009, Icarus, 202, 477
Vernazza P. et al., 2010, Icarus, 207, 800
Vernazza P. et al., 2011, Icarus, 216, 650
Vernazza P. et al., 2015, ApJ, 806, 204
Vernazza P. et al., 2016, AJ, 152, 54
Vokrouhlický D., Bottke W. F., Chesley S. R., Scheeres D. J., Statler T. S., 2015, The Yarkovsky and YORP Effects. p. 509
Walsh K. J., Jacobson S. A., 2015, Asteroids IV, Univ. Arizona Press, Tucson, AZ, p. 375
Walsh K. J., Richardson D. C., Michel P., 2008, Nature, 454, 188
Weidenschilling S. J., 1980, Icarus, 44, 807
Yang B., Zhu J., Gao J., Zhang H. T., Zheng X. Z., 2003, Planet. Space Sci., 51, 411

APPENDIX A: DETAILS ON EACH ASTEROID

A1 (2691) Sérsic

Sérsic is an IMB asteroid, next to the Flora family, near the ν_6 secular resonance, a source region of NEA (Binzel et al. 2004). Average properties of this family are: taxonomic class S (mainly obtained from visible spectroscopy, Florczak et al. 1998) and p_v = 0.305 ± 0.064 (Masiero et al. 2015). From spectroscopic observations of Flora members combined with analyses of meteorite samples, Vernazza et al. (2008), de León et al. (2010), and Dunn et al. (2013) had linked LL chondrite meteorites to the Flora family. No spectrum has been published for (2691) Sérsic previously.

This asteroid was classified as Sr type with a reliability factor of 78.0 per cent (see Popescu et al. 2012, for the details on the reliability factor computation) with a close fit with S and O types. The spectrum shows a shallow absorption feature around 1 μm. Owing to the paucity of known O-type asteroids, and the fact that S types dominate the IMB population (DeMeo & Carry 2013, 2014), we favour an Sr-type classification for Sérsic over a less-likely O type.

From comparison with RELAB data base, the best spectral fit is obtained with Los Angeles meteorite (stone 1, Sample ID:MT-JLB-006-C), a Shergottite, a martian meteorite (basaltic to lherzolitic igneous rocks with chip natural texture). This does not match well with this asteroid, since Shergotittes have an estimated time of 1×10^6 yr (Jagoutz & Wanke 1986), while the Flora family is 1×10^9 yr (Nesvorný et al. 2002). For this reason, we consider the other closer analogues. The second match is for meteorite Hamlet (Sample ID OC-TXH-002-A20), an LL4 ordinary chondrite (OC, Fig.1). The other closer matches are all OC, meteorites: Soko-Banja (OC/LL4, Sample ID MR-MJG-070), Barratta (OC/L4, Sample ID MH-CMP-002), and Bjurbole unshaken (OC/L4, Sample ID MP-FPF-027).

The poor S/N makes the analysis very challenging. Only the NIR part of the spectrum is available, therefore we can compute only the band minima. The first minimum is at 0.9161 ± 0.0054 μm. The spectrum exhibits spectral variations around 1.45 and 1.9 μm due to the influence of telluric water that remained after the data reduction.

We were not able to perform a space weathering analysis on this Sr-type asteroid due to the low S/N data.

A2 (4383) Suruga

This spectrum shows two prominent absorption features at 1 and 2 μm, typical of V-class asteroids, the high S/N of the spectrum ensures a small error in computing band minima. The first minimum is at 0.9254 ± 0.0007 μm and the second minimum is at 1.9710 ± 0.0042 μm which implies a band separation of 1.0456 μm. It can also be seen a weak ∼1.2 μm feature. For basaltic achondrites (BA), this is indicative of the presence of feldspar. The feature is weak in the spectra of howardites (Hardersen, Gaffey & Abell 2004). The normalization of this spectrum was made for the wavelength 1.250 μm.

Only the NIR part of the spectrum is available. We found SDSS observations (Ivezić et al. 2010) and converted them in reflectance (DeMeo & Carry 2013) to complete the spectrum (Fig. 1). We compute a band area ratio (BAR) = 2.6 ± 0.4 and then compute the mafic mineral composition according to Gaffey et al. (2002).

We found W_{O_7} and $F_{S_{45}}$ and the mineral abundances in the olivine-orthopyroxene mixture Ppx/(Opx)+ Ol = 1.1 ± 0.2. We note, however, that although the Band I area is uncertain owing to the poor sampling of the visible part, the BAR we compute is consistent with those of V-type asteroids (Moskovitz et al. 2010).

When analysing with de Sanctis et al. (2011) spectrum of Suruga, the first minimum is at 0.9023±0.0018μm and the second minimum is at 1.8770 ± 0.0072 μm which implies a band separation of 0.9747 μm. Comparing with this work values, there is a notorious difference with the second minima value. This is understandable because De Sanctis spectrum values are noisy around 1.9 μm. In de Sanctis et al. (2011), BII minimum is 1.91 ± 0.005 μm.

Thus, we classified Suruga as a V type (Fig1). Based on its SDSS colours (Ivezić et al. 2001), this minor body was also classified as V type using colours previously (Carvano et al. 2010; Hasselmann, Carvano & Lazzaro 2011; DeMeo & Carry 2013).

When comparing with spectra from RELAB data base, we found spectral matches with the achondrite meteorite Pavlovka, a howardite achondrite (Sample ID:MR-MJG-094). These type of meteorites are thought to have originated from the crust of the asteroid Vesta (Table 3). Other spectra that fits Suruga NIR spectrum corresponds to samples of particulates (0–25 μm) of the meteorites Le Teilleul (Sample ID:MP-TXH-093-A), Frankfort howardite (Sample ID:MP-TXH-085-A), and 'Y-7308,142' (Sample ID:MP-TXH-097-A) all of them Howardite–Eucrite–Diogenite (HED). These matches suggest that the asteroid might be covered by a fine regolith layer. Two other matches corresponds to meteorites Kapoeta P11410 (Sample ID: SN-CMP-012) an achondrite HED Breccia and 'GRO95574,9' (Sample ID: MP-TXH-125) a basaltic HED regolith breccia.

A3 (7187) Isobe

No spectrum has been published previously for (7187) Isobe. We find that (7187) Isobe fits a K-type asteroid with a clear absorption band around 1 μm (Fig. 1) the reliability of the classification is 80.4 per cent. The local minimum around 1 μm was found at 1.0707 μm adjusting a second degree polynomial with $R^2 = 0.8532$. The fits with Xk and Cg types do not show very well this 1 μm feature (Fig.1).

The RELAB sample that best fits is a Particulate Ground Dry-Sieved, Almahata Sitta #4 < 125 μm meteorite (sample ID: MT-PMJ-093-C), an Achondrite Ureilite Anomalous Polymict (0–125 μm). Another fit is with a sample of Allende: HC-10 dark inclusion meteorite, a carbonaceous chondrite (sample ID: MT-TJM-073). Allende meteorite is olivine-rich, and contain an abundant matrix that is relatively featureless in the NIR which explains why the 1μm absorption feature is subtler than in OC spectra (Vernazza et al. 2011). Meteorite Tsarev (sample ID: MA-ATB-053 OC) an OC, also fits this spectrum. Other meteorite spectra found were 'LEW87009,16' (sample ID: LM-LAM-011), 'EET90021,10' (sample ID: MP-TXH-043), and 'LEW87148,15' (sample ID: MP-TXH-016); all of them carbonaceous chondrite. Of the last four spectra the one of 'LEW87009,16' fits better the absorption around 1 μm.

With the uncertainty of (7187) Isobe geometrical albedo $p_v = 0.134 \pm 0.104$ (Masiero et al. 2012), it is hard to favour one solution if CC, OC, and ureilite are together. There is however a clear dichotomy between ureilitic and chondritic materials (Table3). Regarding ureilites, this is consistent with the weak mafic iron silicate absorption bands that this spectrum presents in the 1 and 2 μm region, according to Cloutis et al. (2010). The visible counterpart of the spectrum is needed to complete the analysis.

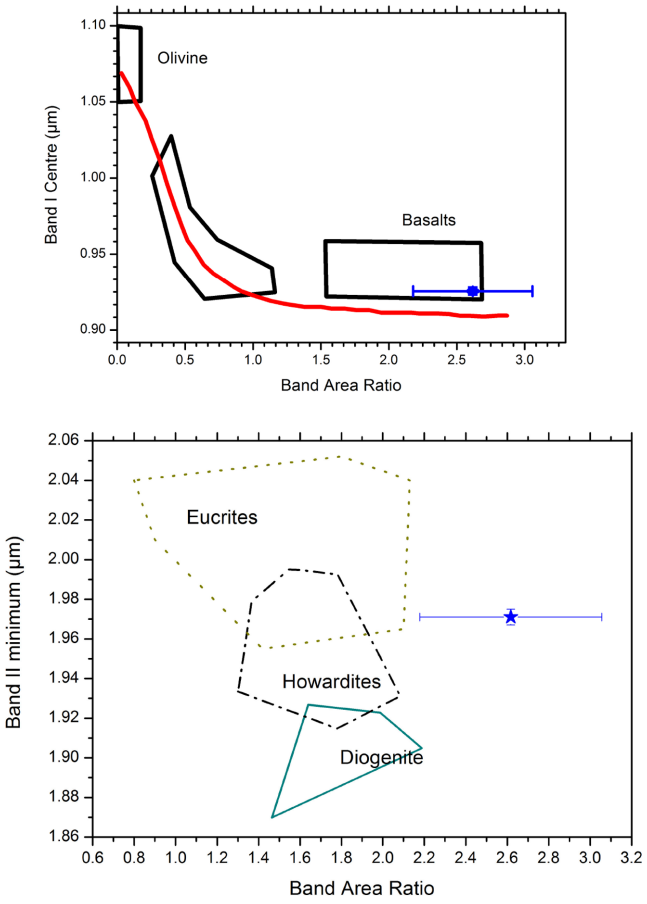

Figure A1. Mineralogical analysis of (4383) Suruga: top*:* BAR versus Band I centres. The regions enclosed by continuous lines correspond to the values for BA, OC, and olivine-rich meteorites (Ol) according to Gaffey et al. (1993). Bottom*:* Suruga spectrum placed into BAR versus Band II minimum HED diagram of Moskovitz et al. (2010). The BAR of Suruga is larger than those represented by HED's similarly as V-type asteroids BARs in Moskovitz et al. (2010).

The spectrum of Isobe shows a complex band around 1 μm and almost no absorption band around 2 μm. This band, usually associated with the presence of olivine, was modelled using Modified Gaussian Model (MGM, Sunshine & Pieters 1993) by fitting multiple Gaussian-like absorption bands (Pieters & McFadden 1994). Indeed, this 1 μmabsorption band is the result of multiple type of absorptions of olivine. Our best fit was obtained using three absorption bands centred at 0.911, 1.041, and 1.235 μm, respectively. The lack of observational data towards 0.7 μm makes problematic the value for the first band used in this model. However, using the two other bands, we can constrain the Fa value (the measure of iron content of olivine) around 20–30 per cent (Nimura et al. 2006).

A4 (8373) Stephengould

This spectrum is featureless (Fig. 1), although it shows some artefacts. The bad signal does not permit to draw more conclusions. A composite VNIR spectrum by de León et al. (2010) was found in the literature and the NIR spectrum in this work has similar trends with it. Into our analysis, we used the visible spectrum of de León et al. (2010), merge it with our NIR data, and compare the results of these two composite spectra. The composite spectral slope is 0.6463 with a correlation of 0.8.

We find that the taxonomic type that better fits the NIR spectrum is X type followed by T and D types with a reliability of 75.6 per cent while when concatenating the visible part of de León et al. (2010) spectrum with our NIR spectrum, the order for the whole VNIR data changes to D, T, and X types with a reliability of 92.6 per cent.

D-type asteroids are characterized by low albedos (Fulchignoni, Birlan & Antonietta Barucci 2000), and are scarce in the inner Solar system (see DeMeo et al. 2014b; Carry et al. 2016). T-type asteroids seems to be also not so representative for the entire asteroidal population (DeMeo & Carry 2014) and could be interpreted as an end-member class. Having no albedo information for Stephengould, and due to the more abundant X-type asteroids (DeMeo & Carry 2013); this asteroid is more akin to the X-complex, although fits better to D type (Fig.1).

Comparing the asteroid VNIR spectrum with RELAB spectra, the best fits are for: the Mixture/10/90 TRO201/MET101 MIX09 (Sample ID: SC-EAC-093), Iron/IA Metal MET101 (Sample ID: SC-EAC-063), Sulfide/Troilite TRO201 <45 μm (Sample ID: EA-EAC-001-B), CC/Heated Unusual CI/CM Tagish Lake heated at 100°C (Vacuum, oxygen eater, 1 week) (Sample ID: MT-TXH-024), and Iron/Finest Octahedrite, Plessitic (0.15 mm) IRANOM Butler (Sample ID: MR-MJG-081).

A5 (76818) 2000 RG_{79}

No spectrum has been published previously for 2000 RG_{79}. The NIR spectrum obtained with SpeX (Fig. 1) has no features, only a very slight absorption at 2 μmand a low slope that turns slightly negative around 2.37 μmuntil the end of the spectrum. We find that the taxonomic types that better fits this spectrum are Xc, Xe, and Ch types (Fig.1). The reliability of the classification is 82.9 per cent. From inspection of these classification, and comparing with Bus DeMeo MITs classification tool, the match that resembles best the spectrum of the asteroid is Xe type, which are numerous among Hungarian (DeMeo & Carry 2014).

When comparing the asteroid spectrum with RELAB samples, the best fits of the spectra were for enstatite chondrite 'ALHA81021,89 (EL6) < 25 μm' (Sample ID: MT-PFV-119-B), Achondrite Mayo Belwa (Sample ID:TB-TJM-046), enstatite chondrite 'QUE93372,13 (EH5) < 25 μm' (Sample ID:MT-PFV-129-B), enstatite chondrite 'ALH84206,25 (EH3) < 45 μm' (Sample ID:MT-PFV-118-A), and enstatite chondrite 'KLE98300,33 (EH3) < 45 μm' (Sample ID:MT-PFV-122-A). The estimated geometric albedo of the featureless spectra of (76818) 2000 RG79 is compatible with enstatite chondrite meteorites (Vernazza et al. 2009).

A6 (190208) 2006 AQ

The S/N of this NIR spectrum is low, but it can be noticed a slight absorption feature at 1 μm. We find that the taxonomic types that better fits this spectrum are K, Cg, and Ch. (Fig.1). The reliability of the classification is 80.4 per cent. From inspection of these classification, the match that resembles best the spectrum of (190208) 2006 AQ is a K type.

When comparing the asteroid spectrum with RELAB samples, the best fits are of different type of meteorites: Igneous meteorite Los Angeles (stone 1) (Sample ID: MT-JLB-006-B), Carbonaceous Chondrite meteorites Murchison (Sample ID: MR-MJG-109), OC meteorites Athens (LL6) chip (Sample ID: OC-TXH-013-A), Chondrite meteorites NWA753 (Sample ID: TB-TJM-114), and Chondrite meteorites A-881988,70 (Sample ID: MP-TXH-059) is obtained.

A7 (348400) 2005 JF_{21}

The NIR spectrum (Fig. 1) shows two prominent absorption features at 1 and 2 μm, typical of V-class asteroids. Evidently, the best match is for V type followed by Sv and Sr types. The reliability of the classification is 82.9 per cent. When computing band minima, the first minimum is at 0.9332 ± 0.0008 μm, and the second minimum at 1.9117 ± 0.031 μm which implies a band separation of 0.9785 μm. Only the NIR part of the spectrum is available, and as such solely the band minima can be computed.

Comparing the asteroid NIR spectrum with RELAB meteorite data base, all the best matches are Achondrites of varied subtypes: meteorite Kapoeta (ID: MP-TXH-053) subtype Basaltic HED Howardite; meteorite 'MIL07001 < 45 μm' (ID: MT-AWB-168-A) subtype Basaltic HED Diogenite Harzburgitic and meteorite 'GRA98108,26 chip' (ID: RM-REM-125) subtype Basaltic HED Olivine–Diogenite are the three best matches.

A8 (399307) 1991 RJ_2

The NIR spectrum (Fig. 1) shows no features and a positive slope of 0.226212 ± 0.005658. The best match for this object is T taxon, followed by X and Xk types. The reliability of the classification is 80.4 per cent.

Comparing the asteroid NIR spectrum with RELAB meteorite data base, the best five matches are for these meteorites: CC/CM2 Mighei meteorite (ID: MA-ATB-072), CC/Laser-Irradiated CM Mighei 4d 75–125 μm meteorite (ID: MA-ATB-065), OC/L6 Pervomaisky meteorite (ID: RS-CMP-064), Sulfide/Troilite Mundrabilla troilite meteorite (ID: MB-CMP-006-P3), and CC/CM2 Murchison meteorite heated at 700C (ID: MB-TXH-064-HD).

A9 1994 XD

The NIR spectrum (Fig. 1) shows clearly an absorption around 0.9 μm. The best match for this feature is for S type, followed by

Table A1. Slopes and mineralogical parameters of the spectra of binaries obtained (when possible) using Cloutis model.

Object	Band I (μm)	Band II (μm)	Band II–Band I (μm)	Slope (1/μm)
(2691) Sérsic	0.9161 ± 0.0054	–	–	0.0633
(4383) Suruga	0.9254 ± 0.0007	1.9710 ± 0.0042	1.0456	0.0616
(7187) Isobe	1.0707	–	–	0.1571
(8373) Stephengould	–	–	–	0.6463
(76818) 2000 RG_{79}	–	–	–	0.0395
(88710) 2001 SL_9	0.9246 ± 0.0038	1.8727 ± 0.0087	0.9481	–
(162483) 2000 PJ_5	0.9591 ± 0.0034	1.9669 ± 0.1805	1.0078	–

Cgh and Ch types, which absorption is shallow at that wavelength. The reliability of the classification is 80.4 per cent.

When computing band parameters, the first minimum is prominent at 0.9196 ± 0.0027 μm, and the second, less noticeable minimum is at 1.7824 ± 0.1305μm, this implies a band separation of 0.8628 μm,. Only this NIR spectrum is available, thus, solely the band minima can be computed for 1994 XD.

Comparing the asteroid NIR spectrum with RELAB meteorite data base, the best five matches are for these meteorites: OC/H5 Barwise (ID: MR-MJG-036), OC/L3.1 LEW86018,71 (L3.1) <45 μm (ID: MT-PFV-130-A), OC/L5 M-L5-15 (Aribba) bulk <125 μm (ID: DP-JNG-017), OC/LL3 Krymka dark powder (ID: RS-CMP-063-D), and OC/L5 Blackwell (ID: MT-HYM-081).

A10 2014 WZ_{120}

The NIR spectrum (Fig. 1) shows clearly absorptions around 1 and 2 μm. The best match for this features is for Sv type, followed by Sr and S types. The reliability of the classification is 80.4 per cent.

When computing band parameters, the first minimum is prominent at 0.9255 ± 0.0007 μm, the second minimum is at 1.8468 ± 0.0128 μm, this implies a band separation of 0.9213 μm. Only this NIR spectrum is available, thus, solely the band minima can be computed.

Comparing the asteroid NIR spectrum with RELAB data base, all the best five matches are for OC and all but Lancon meteorite, which is a H6 Olivine-Bronzite, are subtype H5. These are the meteorites: Ehole chip irradiated with pulse laser at 20 mJ energy x 2 (ID: OC-TXH-006-A40), Zhovtnevyi (ID: MR-MJG-041), Allegan (ID: TB-TJM-125), Magombedze (ID: TB-TJM-108), and Lancon (ID: MR-MJG-033).

A11 (410777) 2009 FD

The NIR data (Fig. 1), although noisy, shows an overall featureless spectrum. The best matches proposed for this spectrum are for the C complex: C, Cb, and Cg types (Fig.1). The reliability of the classification is 82.9 per cent.

Comparing the asteroid NIR spectrum with RELAB data base, the five best matches are: KLE98300,33 (EH3) < 25μm (ID: MT-PFV-122-B), Y-82162,79 <125 μm (ID: MB-CMP-019-A), Almahata Sitta #4 chip lighter face (ID: MT-PMJ-093), EET96135,20 (EH4/5) 45 μm (ID: MT-PFV-120-A), and El-Quss Abu Said (CM2) < 125μm (ID: MP-KHO-131-A).

This asteroid is considered as C type from visible colours in Spoto et al. (2014).

A12 (452561) 2005 AB

This asteroid is classified inside C-complex with a reliability of 80.45 per cent, the most akin to Cb, C, and Xk taxons (Fig. 1). The asteroid exhibit a thermal tail towards 2.5 μm which can help us to estimate its geometrical albedo based on thermal excess approach (Rivkin, Binzel & Bus 2005), a geometrical albedo of 0.03 was estimated from excess of thermal radiation by Kumar, Hardersen & Gaffey (2006). Our computation of the thermal excess parameter gives a value of 0.224 ± 0.011. The asteroid was observed at a distance around 1.1 au having a phase angle around 50°. The computed value of geometrical albedo 0.06 ± 0.02, which makes it compatible with low albedo taxons (C, P, T, or D).

Comparing the asteroid NIR spectrum with RELAB data base, the five best matches are: Almahata Sitta (ID: MT-PMJ-098), Rose City (ID: MR-MJG-079), Abee 900C (ID: MT-TXH-040-F), Y-74659 TXH (ID: MB-TXH-087-C), and Murchison (ID: MH-FPF-052-A). Considering the low albedo of 2005 AB as well as the thermal tail in its spectrum, a mineralogy compatible to dark materials – similar to CC or ureillitic materials – is more probable for this object. Removing the thermal emission of the spectrum, the best match is with Ch, Cgh, and Xk taxons.

A13 (162000) 1990 OS

The spectrum (Fig. 1) is limited to the visible, that wavelength interval already shows the typical S-type curve. We find that the taxonomic types that better fits this spectrum are S, Sv, and L types. The reliability of the classification is 21.9 per cent (low because of the small range considered). Even though, from inspection of this classification, the match that resembles best the spectrum of the asteroid is S type.

Comparing the asteroid visible spectrum with RELAB data base, the five best matches are diverse: AC/Angrite Sahara 99555 (ID: TB-TJM-057), Si/Ol ALHA77005 olivine (ID: DD-MDD-009), CC/CV3 Leoville (ID: MR-MJG-120), CC/CK5-6 EET87860,14 (ID: LM-LAM-012), and Iron/IAB Silicate inclusion Campo de Cielo SI (ID: TB-TJM-059). This is understandable due to the limited data range.

A14 (66063) 1998 RO_1

The best match is for S type – which fits very well the spectrum – followed by Sr and Sv types (Fig.1). The reliability of the classification is 80.4 per cent.

When computing band parameters, the first minimum is at 0.9221 ± 0.0031 μm, and the second minimum is at 1.8525 ± 0.0229 μm, this implies a band separation of 0.9304 μm.

Comparing the asteroid NIR spectrum with RELAB meteorite data base, the best fits for the spectra were all for OC: OC/L5

Malakal (Sample ID: TB-TJM-109), OC/L3 Y-74191 (Sample ID: MB-TXH-084-A), OC/L6 Paranaiba (Sample ID: MB-CMP-010-L), OC/L6 Kuttippuram (Sample ID: TB-TJM-098), and OC/L5 Mirzapur (Sample ID: TB-TJM-111).

A15 (88710) 2001 SL_9

The NIR spectrum (Fig. 1) shows the typical S-type curve. We find that the taxonomic types that better fits this spectrum are Sr, S, and Sq types with a reliability in the classification of 80.4 per cent. From inspection, the match that resembles best the spectrum is Sr type.

This asteroid was classified by Lazzarin et al. (2004, 2005) as Sr and Q types, they also determined an analogue meteorite with VNIR data from *Spectroscopic Investigation of Near Earth Objects* (Lazzarin, Magrin & Marchi 2008).[8] de León et al. (2010) classify it as Q type. Lazzarin et al. (2008) NIR data have low S/N, for this work we had use their visible spectrum (available in `M4AST` libraries) and join it with the NIR spectrum to perform the analysis. Fig. A2 shows the VNIR composite spectrum we used to analyse with Cloutis model.

The position of the centre of the two absorption bands were computed, their values are: BI min[μm] = 0.9246 ± 0.0038, BII min[μm] = 1.8727 ± 0.0087, and band separation[μm] = 0.9481. The band centres are: BI centre[μm] = 0.9357 ± 0.0042, BII centre[μm] = 1.8721 ± 0.0086, and the BAR: 0.5858 ± 0.0019.

From our analysis, the resultant mineralogy is OPX/(OPX+OL)[μm] = 0.2976 (Fig. A2). This means that 2001 SL_9 is an OC, more akin to L subtype.

Comparing the asteroid VNIR spectrum with RELAB samples, the best fits are all for OC: OC/LL4 Hamlet (LL4) <125 μm (Sample ID: OC-TXH-002-C), OC/L6 Chateau Renard (L6) <125 μm pellet irradiated with 5 mJ + 10 mJ laser (Sample ID: OC-TXH-011-D15), OC/H3.4 Chondrule M-H3.4-2149C (Dhajala H3.4) chondrules <125 μm (Sample ID: DP-JNG-012), OC/L5 Tsarev 15384,3-2 (Sample ID: RS-CMP-065-T), and OC/L4 Saratov (Sample ID: MB-CMP-028-B).

A16 (162483) 2000 PJ_5

Polishook & Brosch (2008) obtained all the characteristics of this Aten asteroid, they even estimate its taxonomy from phase curve parameters, using the correlation between phase and albedo found by Belskaya & Shevchenko (2000).

Even though the NIR spectrum (Fig. 1) is somehow noisy, the obtained data clearly show absorption features at 1 and 2 μm. We find that the taxonomic types that better fits this spectrum are Q, K, and S. The reliability of the classification is 82.9 per cent. From inspection of these classifications, the match that resembles best the spectrum is a Q type.

The first minimum is at 0.9591 ± 0.0034 μm and the second minimum is at 1.9669 ± 0.1805 μm which implies a band separation of 1.0078 μm.

Comparing the asteroid spectrum with RELAB samples, the best fits of the spectra were for OC: OC/H4 Quenggouk (Sample ID: MR-MJG-042), OC/LL6 Bandong (Sample ID: TB-TJM-067), OC/ll6 Amphoterite Jelica (Sample ID: MR-MJG-072), OC/L6 Olivine-Hypersthene Leedey (Sample ID: MR-MJG-060), and OC/LL6 NWA1948 (LL6) <250 μm (Sample ID: OC-SXS-023-D).

[8] http://www.astro.unipd.it/planets/sineo.html

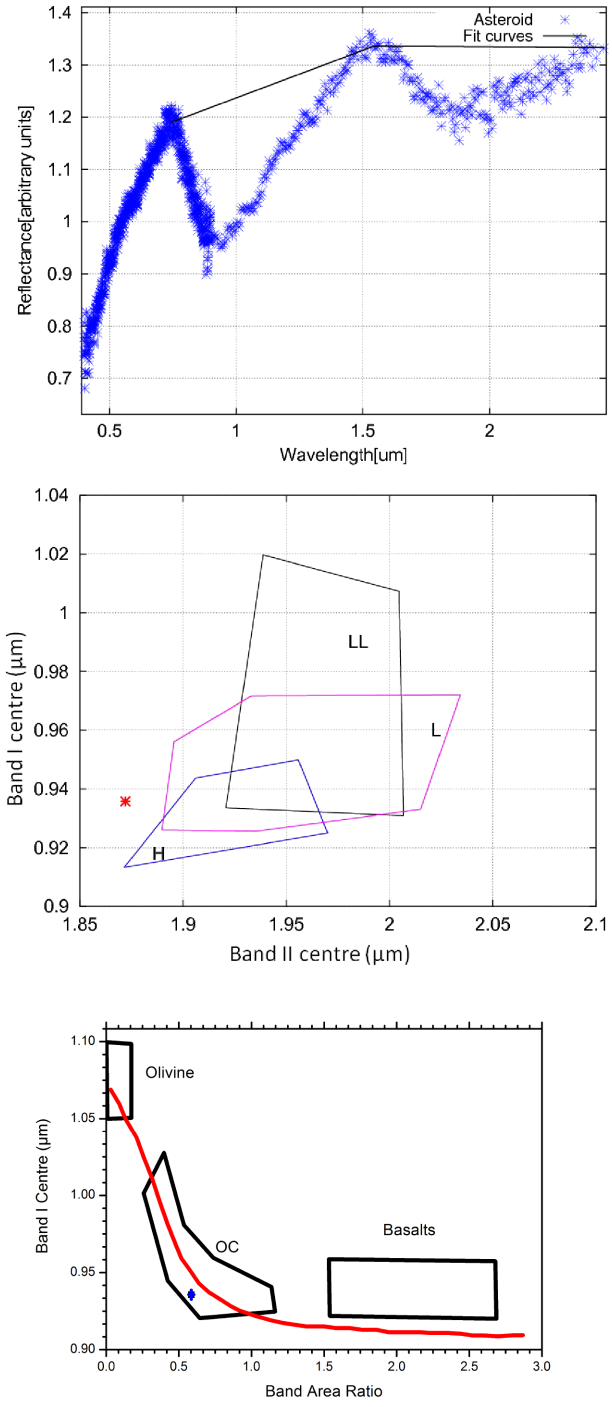

Figure A2. Mineralogical analysis results for (88710) 2001 SL_9. Top: linear continuum tangential to spectral curve of spectrum obtained after merging visible spectrum (Lazzarin et al. 2004) and NIR spectrum of (88710) 2001 SL_9. Middle: wavelength position of the centres of the two absorption bands. The regions enclosed correspond to the band centres computed for the H, L, and LL chondrites. Bottom: BAR versus Band I centre. The regions enclosed by continuous lines correspond to the values computed for BA, OC, and olivine-rich meteorites (Ol) (Gaffey et al. 1993).

This asteroid was already classified by Thomas et al. (2014) and DeMeo et al. (2014a) as Q type, and as O type by de León et al. (2010).

A17 (374851) 2006 VV_2

For this asteroid, colour indices were measured by Betzler & Novaes (2009): $(B-V)=0.84$, $(V-R)=0.39\pm0.02$, and $(B-R)=1.23$; Hergenrother, Whiteley & Christensen (2009), and Vereshchagina et al. (2009), who reported a strong dependence of the shape of the light curve on the colour.

This spectrum was published by Reddy (2009, Fig.1). Although no taxonomy has been published (in peer-reviewed journals), several taxonomies had been proposed before: from SpeX data: V (Howell et al. 2008); from colour indices: S type (Hergenrother et al. 2009), A type (Vereshchagina et al. 2009; Vereshchagina 2011), and V, Q, or T type (Betzler & Novaes 2009).

The best matches are for L, Xe, and Ch types with a reliability of 90 per cent. However, this spectrum has good S/N and clearly shows absorption features around 1 and 2 μm that are shallow for the proposed taxonomies around 1 μm, and non-existent around 2 μm. M4AST has a feature that allows comparison of the spectrum with different types from Bus–DeMeo taxonomy; using it, and after visual inspection looking for a good fit of the band positions and shapes, we found that the best matches are for Sr and S types (the best matches do not necessarily correspond to the lowest χ^2 values).

When computing band parameters, the first minimum is at 0.9201 ± 0.0013 μm, and the second minimum at 1.9498 ± 0.0037 μm which implies a band separation of 1.0297 μm. Only this NIR spectrum is available, thus, solely the band minima can be computed for (374851) 2006 VV2.

Comparing the asteroid NIR spectrum with RELAB data base, the best matches are: OC/L5 Olivine-Hypersthene meteorite Farmington (ID: MR-MJG-077) Achondrite Ureilite Anomalous Polymict Almahata Sitta #51 chip (ID: MT-PMJ-110), OC H3.4 M-H3.4-2149 (Dhajala H3.4) bulk <125 μm(ID: DP-JNG-011), OC H5.6 Novosibirsk dark fraction (ID: RS-CMP-049-L), and OC H3.7 ALH85121,11 (H3.7) <45 μm(ID: MT-PFV-154-A).

A18 (399774) 2005 NB_7

This NIR spectrum shows clearly an absorption around 0.9 μm and a slightly shallow absorption around 2 μm. The best match is for Sq type followed by S and Q types (Fig. 1). The reliability of the classification is 82.9 per cent. However, the band parameters could not be computed with the tool, by means of a polynomial adjustment we estimate 0.95 μm for the first minimum.

Comparing the asteroid NIR spectrum with RELAB data base, the best matches are for different type of meteorites: OC/L6 Chateau Renard (L6) <125 μm pellet irradiated with 5 mJ + 10 mJ + 20 mJ laser (ID: OC-TXH-011-D35), Igneous/Shergottite EETA79001,73 (ID: LM-LAM-007-73), CC/C3 Ungrouped LEW85332,48 (ID: MT-EKT-017), OC/LL6 Appley Bridge (LL6) chip pulse-laser irradiated with 20 mJ x 2 (ID: OC-TXH-012-A40), and OC/L5 Tsarev 15384,3-2 (ID: RS-CMP-065-T).

2005 NB_7 has been previously identified as Sq type in Gietzen et al. (2012) with SpeX data using the MGM (Sunshine & Pieters 1993).

A19 2007 DT_{103}

The best matches for this spectrum (Fig. 1) are for Q, Sq, and S types. From all of these, Q type matches beautifully. When computing band parameters, the first minimum is prominent at 0.9670 ± 0.0047 μm, and the second, less noticeable minimum, is at 1.9652 ± 0.0128 μm, this implies a band separation of 0.9982 μm,

Comparing the asteroid NIR spectrum with RELAB data base, the best fits for the spectrum were for: Laser-Irradiated OC Chateau Renard (L6) chip pulse-laser irradiated with 20 mJ x 4 (Sample ID: OC-TXH-011-A80), Achondrite Almahata Sitta #44 125–500 μm (Sample ID: MT-PMJ-108-B), OC Y-74442 (Sample ID: MB-TXH-086-A), OC Appley Bridge (LL6) chip pulse-laser irradiated with 20 mJ x 2 (Sample ID: OC-TXH-012-A40), and OC Y-74646 (Sample ID: MB-TXH-085-B). From all these meteorites, the best match for a meteorite spectrum is for Almahata Sitta.

This asteroid was already classified as a potential Q type in DeMeo et al. (2014b).

A20 (8306) Shoko

From our analysis of this spectrum (Fig. 1), Shoko is a Q type; Sq and S are also proposed, this classification has a reliability of 80.4 per cent. When computing band parameters, the first minimum is at 0.9873 ± 0.0085 μm, and the second minimum is at 2.0344 ± 0.0078 μm, this implies a band separation of 1.0471 μm.

Comparing the asteroid NIR spectrum with RELAB meteorite data base, the best fits for the spectra were for OC: Quenggouk (Sample ID: MR-MJG-042), Jelica (Sample ID: MR-MJG-072), Greenwell Springs (Sample ID: TB-TJM-075), Chateau Renard (L6) chip pulse-laser irradiated with 20 mJ energy (Sample ID: OC-TXH-011-A20), and NWA1799 (LL5) <250 μm (Sample ID: OC-SXS-026-D).

Polishook et al. (2014) classified Shoko as Sq type using PCA on NIR spectrum obtained at IRTF/SpeX, completing the visible part with *BVRI* colours. From that analysis, Shoko presents a fresh surface.

A21 (185851) 2000 DP_{107}

Colour indices has been measured by Pravec et al. (2000) $(U-B)$: 0.278, $(B-V)$: 0.70, $(V-R)$: 0.388 ± 0.013, $(B-R)$: 1.088 ± 0.019, $(V-I)$: 0.717, and Dandy, Fitzsimmons & Collander-Brown (2003) $(B-V)$: 0.667 ± 0.033, $(V-R)$: 0.405 ± 0.019, $(V-I)$: 0.687 ± 0.024, and $(V-Z)$: 0.799 ± 0.056.

The best proposed matches are for Xk, Cg, Cb, Ch, and K types (Fig. 1), a classification with a reliability of 80.4 per cent. From inspection, there is an absorption band not considered in X or C types. Thus, the most resemblance is to K type with thermal effect.

Comparing the asteroid NIR spectrum with RELAB meteorite data base, the best fits for the spectra are: Carbonaceous Chondrite PCA02012 (Sample ID: PH-D2M-044), OC Gorlovka (Sample ID: RS-CMP-048), OC Orvinio Clast and Melt (Sample ID: MP-DTB-028-C), Carbonaceous Chondrite MET00426 (Sample ID: PH-D2M-055), and Achondrite Almahata Sitta #4 chip lighter face (Sample ID: MT-PMJ-093). From all these, the best match between spectra is for meteorite Gorlovka.

Previous classifications are: C type from colour indices (Pravec et al. 2000; Dandy et al. 2003) and from Yang et al. (2003) X type based on visible spectrum and albedo.

We concatenate the visible spectrum from Yang et al. (2003) with the NIR spectrum. After performing the match with RELAB data

base found these samples: Allende 700C (Sample ID: MB-TXH-063-HD), Tsarev >300 μm (ground) (Sample ID: MA-ATB-053), Orvinio Clast & Melt (Sample ID: MP-DTB-028-C), DaG 1042,05 <125 μm (Sample ID: LM-H1T-052-C), and Abee 700C (Sample ID: MT-TXH-040-D). From these, the best match is for Tsarev meteorite.

A22 (153591) 2001 SN_{263}

This spectrum has not features, it is C-like. The best match is for C type followed by Cb and Cg types (Fig. 1). The reliability of the classification is 82.9 per cent.

Comparing the asteroid NIR spectrum with RELAB data base, the best fits for the spectrum are: Almahata Sitta #4 chip lighter face (Sample ID: MT-PMJ-093), El-Quss Abu Said (CM2) <125 μm (Sample ID: MP-KHO-131-A), EET96135,20 (EH4/5) <25 μm (Sample ID: MT-PFV-120-B), Y-82162,79 <125 μm (Sample ID: MB-CMP-019-A), and KLE98300,33 (EH3) <25 μm (Sample ID: MT-PFV-122-B).

A previous classification of this binary was performed by Perna et al. (2014) who found it to be B type.

A23 (285263) 1998 QE_2

Even though this spectrum has a low S/N, it can be seen that there are no typical absorptions of S, or Q types. The best match is for X type followed by T and D types (Fig.1). The reliability of the classification is 80.4 per cent.

Comparing the asteroid NIR spectrum with RELAB meteorite data base, the best fits for the spectrum are: Meghei (Mighei) (Sample ID: MR-MJG-108), TRO201 (Sample ID: SC-EAC-064), Mundrabilla troilite (Sample ID: MB-CMP-006-P2), Tagish Lake (Sample ID: MT-MEZ-011), and Allende (Sample ID: MS-CMP-040-C).

Previous Ch classification was performed by Hicks, Buratt & Dalba (2013a) and Hicks et al. (2013b), their visible data were used by Moskovitz et al. (2017) who included NIR Spex data in an analysis of the aspect dependent variability of (285263) 1998 QE_2 spectrum with thermal tail.

While the best taxonomic classification of this object is in favour of puzzling classes such as T and D, into our mineralogical analysis, we cannot omit the case of materials which are not obviously presented into the meteorite collections. Indeed, friable, fragile, or rich volatile bodies have null or less chances to be present in collections of extraterrestrial material. These hypothesis are also supported by recent comparative planetology studies between spectra of asteroids and interplanetary dust particles (Vernazza et al. 2015). Thus, our spectral match with RELAB data should be considered as tentative.

A24 (481532) 2007 LE

The best match we found is for D type followed by X and T types (Fig. 1). From all comparisons, D type fits best the spectrum, although it shows a slight absorption $\sim$ 1 μm. The reliability of the classification is 82.9 per cent.

Comparing the asteroid NIR spectrum with RELAB meteorite data base, the best fits for the spectra are: Stony Iron 'Y-8451,20' (Sample ID: MB-TXH-039), Metal-type Metal in ALH84019 (Sample ID: TB-TJM-056), the type Sulfide Troilite (Sample ID: MI-CMP-011), Mixture MIX09 (Sample ID: SC-EAC-093), and Carbonaceous Chondrite Mighei Separates (Sample ID: MS-CMP-001-D); although neither shows that absorption at 1 μm.

Fieber-Beyer et al. (2015) have performed a complete analysis of an SpeX spectra of 2007 LE, but their spectra shows clearly an absorption around 2 μm and is very red, they applied also a thermal correction. They conclude that the meteoritic analogue is Rose City meteorite which could be a fragment of H Chondrite parent body (6) Hebe, this implies that 2007 LE is more akin to S type according to that work. However, the idea that Hebe is the unique parent body of H chondrites is still under debate. Nedelcu et al. (2014) suggest that there might be at least another H chondrite parent body in the Main Belt and more recently, Marsset et al. (2017) showed that Hebe is unlikely the parent body of OC.

This paper has been typeset from a TEX/LATEX file prepared by the author.

List of astronomical key words (Updated on 2017 March)

This list is common to *Monthly Notices of the Royal Astronomical Society, Astronomy and Astrophysics*, and *The Astrophysical Journal*. In order to ease the search, the key words are subdivided into broad categories. No more than *six* subcategories altogether should be listed for a paper.

The subcategories in boldface containing the word 'individual' are intended for use with specific astronomical objects; these should never be used alone, but always in combination with the most common names for the astronomical objects in question. Note that each object counts as one subcategory within the allowed limit of six.

The parts of the key words in italics are for reference only and should be omitted when the keywords are entered on the manuscript.

General
editorials, notices
errata, addenda
extraterrestrial intelligence
history and philosophy of astronomy
miscellaneous
obituaries, biographies
publications, bibliography
sociology of astronomy
standards

Physical data and processes
acceleration of particles
accretion, accretion discs
asteroseismology
astrobiology
astrochemistry
astroparticle physics
atomic data
atomic processes
black hole physics
chaos
conduction
convection
dense matter
diffusion
dynamo
elementary particles
equation of state
gravitation
gravitational lensing: micro
gravitational lensing: strong
gravitational lensing: weak
gravitational waves
hydrodynamics
instabilities
line: formation
line: identification
line: profiles
magnetic fields
magnetic reconnection
(magnetohydrodynamics) MHD
masers
molecular data
molecular processes
neutrinos
nuclear reactions, nucleosynthesis, abundances
opacity
plasmas
polarization
radiation: dynamics
radiation mechanisms:general
radiation mechanisms: non-thermal
radiation mechanisms: thermal
radiative transfer
relativistic processes
scattering
shock waves
solid state: refractory
solid state: volatile
turbulence
waves

Astronomical instrumentation, methods and techniques
atmospheric effects
balloons
instrumentation: adaptive optics
instrumentation: detectors
instrumentation: high angular resolution
instrumentation: interferometers
instrumentation: miscellaneous
instrumentation: photometers
instrumentation: polarimeters
instrumentation: spectrographs
light pollution
methods: analytical
methods: data analysis
methods: laboratory: atomic
methods: laboratory: molecular
methods: laboratory: solid state
methods: miscellaneous
methods: numerical
methods: observational
methods: statistical
site testing
space vehicles
space vehicles: instruments
techniques: high angular resolution
techniques: image processing
techniques: imaging spectroscopy
techniques: interferometric
techniques: miscellaneous
techniques: photometric
techniques: polarimetric
techniques: radar astronomy
techniques: radial velocities
techniques: spectroscopic
telescopes

Astronomical data bases
astronomical data bases: miscellaneous
atlases
catalogues
surveys
virtual observatory tools

Astrometry and celestial mechanics
astrometry
celestial mechanics
eclipses
ephemerides
occultations
parallaxes
proper motions
reference systems
time

The Sun
Sun: abundances
Sun: activity
Sun: atmosphere
Sun: chromosphere
Sun: corona
Sun: coronal mass ejections (CMEs)
Sun: evolution
Sun: faculae, plages
Sun: filaments, prominences
Sun: flares
Sun: fundamental parameters
Sun: general
Sun: granulation
Sun: helioseismology
Sun: heliosphere
Sun: infrared
Sun: interior
Sun: magnetic fields
Sun: oscillations
Sun: particle emission
Sun: photosphere
Sun: radio radiation
Sun: rotation
(Sun:) solar–terrestrial relations
(Sun:) solar wind
(Sun:) sunspots
Sun: transition region
Sun: UV radiation
Sun: X-rays, gamma-rays

Planetary systems
comets: general

comets: individual: . . .
Earth
interplanetary medium
Kuiper belt: general

Kuiper belt objects: individual: . . .
meteorites, meteors, meteoroids
minor planets, asteroids: general

minor planets, asteroids: individual: . . .
Moon
Oort Cloud
planets and satellites: atmospheres
planets and satellites: aurorae
planets and satellites: composition
planets and satellites: detection
planets and satellites: dynamical evolution and stability
planets and satellites: formation
planets and satellites: fundamental parameters
planets and satellites: gaseous planets
planets and satellites: general

planets and satellites: individual: . . .
planets and satellites: interiors
planets and satellites: magnetic fields
planets and satellites: oceans
planets and satellites: physical evolution
planets and satellites: rings
planets and satellites: surfaces
planets and satellites: tectonics
planets and satellites: terrestrial planets
planet–disc interactions
planet–star interactions
protoplanetary discs
zodiacal dust

Stars
stars: abundances
stars: activity
stars: AGB and post-AGB
stars: atmospheres
(stars:) binaries *(including multiple)*: close
(stars:) binaries: eclipsing
(stars:) binaries: general
(stars:) binaries: spectroscopic
(stars:) binaries: symbiotic
(stars:) binaries: visual
stars: black holes
(stars:) blue stragglers
(stars:) brown dwarfs
stars: carbon
stars: chemically peculiar
stars: chromospheres
(stars:) circumstellar matter
stars: coronae
stars: distances
stars: dwarf novae
stars: early-type
stars: emission-line, Be
stars: evolution
stars: flare
stars: formation
stars: fundamental parameters
(stars:) gamma-ray burst: general
(stars:) **gamma-ray burst: individual: . . .**
stars: general
(stars:) Hertzsprung–Russell and colour–magnitude diagrams
stars: horizontal branch
stars: imaging
stars: individual: . . .
stars: interiors

stars: jets
stars: kinematics and dynamics
stars: late-type
stars: low-mass
stars: luminosity function, mass function
stars: magnetars
stars: magnetic field
stars: massive
stars: mass-loss
stars: neutron
(stars:) novae, cataclysmic variables
stars: oscillations *(including pulsations)*
stars: peculiar *(except chemically peculiar)*
(stars:) planetary systems
stars: Population II
stars: Population III
stars: pre-main-sequence
stars: protostars
(stars:) pulsars: general
(stars:) **pulsars: individual: . . .**
stars: rotation
stars: solar-type
(stars:) starspots
stars: statistics
(stars:) subdwarfs
(stars:) supergiants
(stars:) supernovae: general
(stars:) **supernovae: individual: . . .**
stars: variables: Cepheids
stars: variables: Scuti
stars: variables: general
stars: variables: RR Lyrae
stars: variables: S Doradus
stars: variables: T Tauri, Herbig Ae/Be
(stars:) white dwarfs
stars: winds, outflows
stars: Wolf–Rayet

Interstellar medium (ISM), nebulae
ISM: abundances
ISM: atoms
ISM: bubbles
ISM: clouds
(ISM:) cosmic rays
(ISM:) dust, extinction
ISM: evolution
ISM: general
(ISM:) HII regions
(ISM:) Herbig–Haro objects

ISM: individual objects: . . .
(except planetary nebulae)
ISM: jets and outflows
ISM: kinematics and dynamics
ISM: lines and bands
ISM: magnetic fields
ISM: molecules
(ISM:) photodissociation region (PDR)
(ISM:) planetary nebulae: general
(ISM:) **planetary nebulae: individual: . . .**
ISM: structure
ISM: supernova remnants

The Galaxy
Galaxy: abundances
Galaxy: bulge
Galaxy: centre
Galaxy: disc
Galaxy: evolution
Galaxy: formation
Galaxy: fundamental parameters
Galaxy: general
(Galaxy:) globular clusters: general
(Galaxy:) **globular clusters: individual: . . .**
Galaxy: halo
Galaxy: kinematics and dynamics
(Galaxy:) local interstellar matter
Galaxy: nucleus
(Galaxy:) open clusters and associations: general
(Galaxy:) **open clusters and associations: individual: . . .**
(Galaxy:) solar neighbourhood
Galaxy: stellar content
Galaxy: structure

Galaxies
galaxies: abundances
galaxies: active
(galaxies:) BL Lacertae objects: general
(galaxies:) **BL Lacertae objects: individual: . . .**
galaxies: bulges
galaxies: clusters: general

galaxies: clusters: individual: . . .
galaxies: clusters: intracluster medium
galaxies: distances and redshifts
galaxies: dwarf
galaxies: elliptical and lenticular, cD
galaxies: evolution
galaxies: formation
galaxies: fundamental parameters
galaxies: general
galaxies: groups: general

galaxies: groups: individual: . . .
galaxies: haloes
galaxies: high-redshift

galaxies: individual: . . .
galaxies: interactions
(galaxies:) intergalactic medium
galaxies: irregular
galaxies: ISM
galaxies: jets
galaxies: kinematics and dynamics
(galaxies:) Local Group
galaxies: luminosity function, mass function
(galaxies:) Magellanic Clouds
galaxies: magnetic fields
galaxies: nuclei
galaxies: peculiar
galaxies: photometry
(galaxies:) quasars: absorption lines
(galaxies:) quasars: emission lines
(galaxies:) quasars: general

(galaxies:) **quasars: individual: . . .**
(galaxies:) quasars: supermassive black holes
galaxies: Seyfert
galaxies: spiral
galaxies: starburst
galaxies: star clusters: general

galaxies: star clusters: individual: . . .
galaxies: star formation
galaxies: statistics
galaxies: stellar content
galaxies: structure

Cosmology
(cosmology:) cosmic background radiation
(cosmology:) cosmological parameters
(cosmology:) dark ages, reionization, first stars
(cosmology:) dark energy
(cosmology:) dark matter
(cosmology:) diffuse radiation
(cosmology:) distance scale
(cosmology:) early Universe
(cosmology:) inflation
(cosmology:) large-scale structure of Universe
cosmology: miscellaneous
cosmology: observations
(cosmology:) primordial nucleosynthesis
cosmology: theory

Resolved and unresolved sources as a function of wavelength
gamma-rays: diffuse background
gamma-rays: galaxies
gamma-rays: galaxies: clusters
gamma-rays: general
gamma-rays: ISM
gamma-rays: stars
infrared: diffuse background
infrared: galaxies
infrared: general
infrared: ISM
infrared: planetary systems
infrared: stars
radio continuum: galaxies
radio continuum: general
radio continuum: ISM
radio continuum: planetary systems
radio continuum: stars
radio continuum: transients
radio lines: galaxies
radio lines: general
radio lines: ISM
radio lines: planetary systems
radio lines: stars
submillimetre: diffuse background
submillimetre: galaxies
submillimetre: general
submillimetre: ISM
submillimetre: planetary systems
submillimetre: stars
ultraviolet: galaxies
ultraviolet: general
ultraviolet: ISM
ultraviolet: planetary systems
ultraviolet: stars
X-rays: binaries
X-rays: bursts
X-rays: diffuse background
X-rays: galaxies
X-rays: galaxies: clusters
X-rays: general
X-rays: individual: . . .
X-rays: ISM
X-rays: stars